THESIS

THE EFFECTS OF AMBIENT AIR-INJECTION ON PARTICULATE MATTER EMISSIONS IN HIGH FIREPOWER CHIMNEY COOKSTOVES

Submitted by

Thor Hogberg

Department of Mechanical Engineering

In partial fulfillment of the requirements

For the Degree of Master of Science

Colorado State University

Fort Collins, Colorado

Spring 2017

Master's Committee:

Advisor: Anthony Marchese

Christian L'Orange
Jeffrey Collett Jr.
Shantanu Jathar

ABSTRACT

THE EFFECTS OF AMBIENT AIR-INJECTION ON PARTICULATE MATTER EMISSIONS IN HIGH FIREPOWER CHIMNEY COOKSTOVES

Approximately 2.8 billion people use solid fuel to cook and heat their homes. The resulting emissions from using solid fuel to cook and heat has detrimental effects on both indoor and outdoor air quality. In 2012 it was estimated that 4.3 million premature deaths occurred from indoor air pollution and 3.7 million deaths occurred from ambient air pollution. In 2009 it was estimated that incomplete combustion and harvesting of solid biofuels combined accounted for 1.9-2.3% of all greenhouse gases and short lived climate forcers. Due to the high firepower of institutional stoves, they produce far greater amounts of particulate matter (PM) than residential cookstoves; despite this fact, they have received little attention in comparison.

Technology at the Advanced Biomass Combustion Laboratory has been developed that is capable of reducing PM emissions in high firepower chimney stoves by over 90%, and shifting the elemental to organic carbon ratio (EC/OC) towards a higher organic fraction. These changes were achieved by the use of high velocity air injection directly above the combustion chamber. Air injection nozzle orifice number, diameter, and the mass flow rate of injection air was tested to understand what combination of geometry and flow rate resulted in the best overall emissions reduction. The most significant emissions reductions occurred at high velocities that resulted from nozzles with fewer and smaller holes.

ACKNOWLEDGEMENTS

The unending love and support I have received from my family has given me the patience to make it through graduate school. Without their support I would not have been able to make this small contribution to a very big obstacle. Aside from my family, I thank all of my fellow "Stovies." Our constant collaboration has been a learning experience of its own, and rewarded me with unparalleled experience. Outside the stoves community, there are a lot of people at the Engines & Energy Conversion Lab who played some role in the work completed in this investigation who also receive my thanks.

Thanks to the Global Alliance for Clean Cookstoves (GACC), who awarded CSU's Advanced Biomass Combustion Laboratory with the pilot innovation fund (PIF) that made this work possible.

TABLE OF CONTENTS

LIST OF TABLES

LIST OF FIGURES

1 INTRODUCTION

Humans have been using fire for many thousands of years, but only in recent history recognized the benefit of removing smoke from the home. There is evidence of in-home ventilation dating back to the Western Han Dynasty (206 BC – 9 AD) (Pheng, 2004). In western civilization there is record of chimneys being destroyed in Venice by an earthquake in 1347 (Butler, n.d.). In medieval times, homes had a centrally located hearth with a vent in the roof directly above the hearth for smoke to escape. Such vents did help smoke escape to the outdoors, but did not draft smoke up and out of the chimney the way modern chimneys do. Notice in Figure 1 that the top of the hearth is black from soot that constantly escapes into the room rather than being properly drafted up through the "chimney."

Figure 1: Medieval Hearth (Morgan, n.d.)

Ancient China paid a great deal of attention to chimney design (Pheng, 2004), but in the western world it wasn't until the 1700's that the chimney was considered a device worthy of improvement; Benjamin Franklin published "Observations on the Causes and Cure of Smoky Chimneys" (Butler, n.d.). Franklin was responsible for the Pennsylvanian Fireplace and the Franklin Stove, two chimney stoves that were well adopted before the American Revolution. At

this point in history caloric theory reigned as the dominant understanding of heat transfer. Caloric theory suggests that heat is a weightless fluid that can be transferred from warm bodies to cooler ones. One of the first people to disprove the caloric theory, an American-British physicist named Benjamin Rumford, was responsible for the "smokeless chimney," and the "Rumford Fireplace" at about the same time Franklin made his developments with chimney stoves (Butler, n.d.). It may be postulated that caloric theory and the misunderstanding of heat transfer were partially responsible for the slow advance of chimney technology. With heat being understood as a fluid, and also synonymous with the smoke, emissions were gladly allowed into dwellings to keep the occupants warm (Butler, n.d.). According to caloric theory, heat, as a fluid, could only flow from warm to cold. So, smoke couldn't exit a home until the home was sufficiently warm (Butler, n.d.).

Figure 2: Modern Envirofit plancha style chimney stove being installed in a home

Chimney stoves are now used throughout the world in both developed and developing nations for home heating and cooking. Although modern chimneys have far advanced from their medieval predecessors, they do not fully address the problems that arise from the emissions that they remove from the home. This research is motivated by the fact that emissions from burning solid biofuels are incredibly harmful to human health, and a major contributor to both greenhouse gas (GHG) emissions and short lived climate forcers (SLCF). Approximately 2.8 billion people still use solid biomass (wood, charcoal, animal dung, etc.) as a fuel for cooking, lighting, and/or space heating (World Health Organization, 2015).

It is estimated that incomplete combustion and unsustainable harvesting of solid biofuels together contributed 1.9-2.3% of global GHG and SLCF emissions in 2009 (Bailis, Drigo, Ghilardi, & Masera, 2015). In 2012, 4.3 million and 3.7 million premature deaths were linked to household air pollution (HAP) and ambient air pollution (AAP), respectively (World Health Organization, 2015). The majority of these deaths occur in the developing world, where solid biomass is used for cooking and heating. The range of health effects is substantial with the most deaths attributed to ischemic heart disease (IHD), chronic obstructive pulmonary disease (COPD), and stroke (Figure 3) (WHO, 2014). These health effects are a result of fine particles (less than 2.5 μm in aerodynamic diameter) being deposited deep in the lungs. These smaller particles deposit deep in the lungs because they stay entrained in the airflow and then settle in the alveolar region of the lungs (Hinds, 1999).

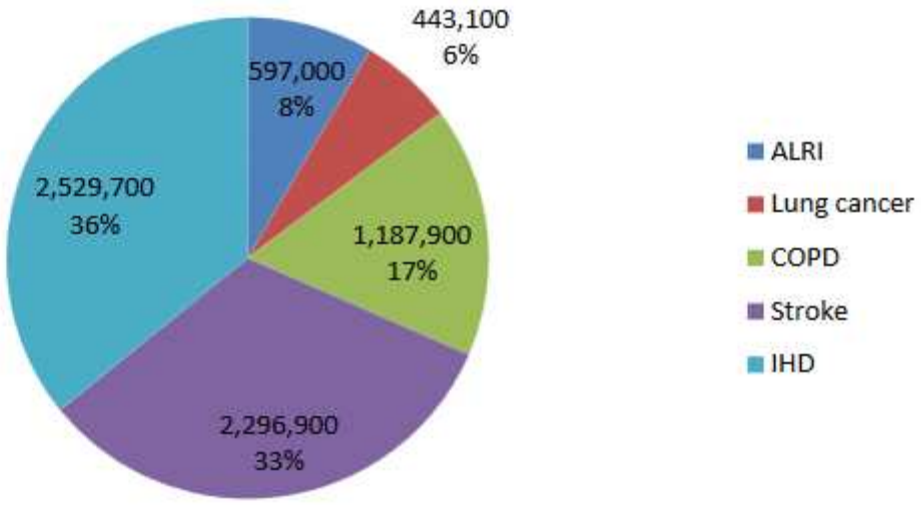

Figure 3: Deaths attributable to the joint effects of HAP and AAP in 2012, by disease (WHO,2014)

These health implications disproportionately affect women and the children they take care of, who spend 11-14 hours a day taking care of the home and cooking (Global Alliance for Clean Cookstoves, 2016). Not only are they constantly exposed to the harmful emissions produced from cooking/heating, but there are also several unhealthy and sometimes dangerous indirect effects caused by the use of biomass. Women are typically responsible for gathering (with the help of the children) or buying fuel (WHO, 2006). Gathering fuel can be dangerous where fuel sources have been depleted, and can sometimes take hours. While gathering fuel many people suffer from broken bones, back aches, and snake bites (WHO, 2006). In war zones and refugee camps there have been reports of women and girls being assaulted while gathering fuel, as a result of leaving the safety of their home (WHO, 2006). Biomass as a fuel source is also a major contributor to deforestation, land degradation, and desertification (WHO, 2006). The constant need for solid fuel perpetuates deforestation and the loss of complex ecosystems,

which then perpetuates the harmful effects that solid fuels have on the climate and the environment because the forest is no longer present to act as a carbon sink.

Cookstoves can also be damaging to the environment. Climate change, commonly referred to as "global warming," is a shift in the global climate that has occurred over the past hundred years. The growth in human population and industrialization resulted in a dramatic increase in the amount of carbon dioxide (CO_2) in the atmosphere.

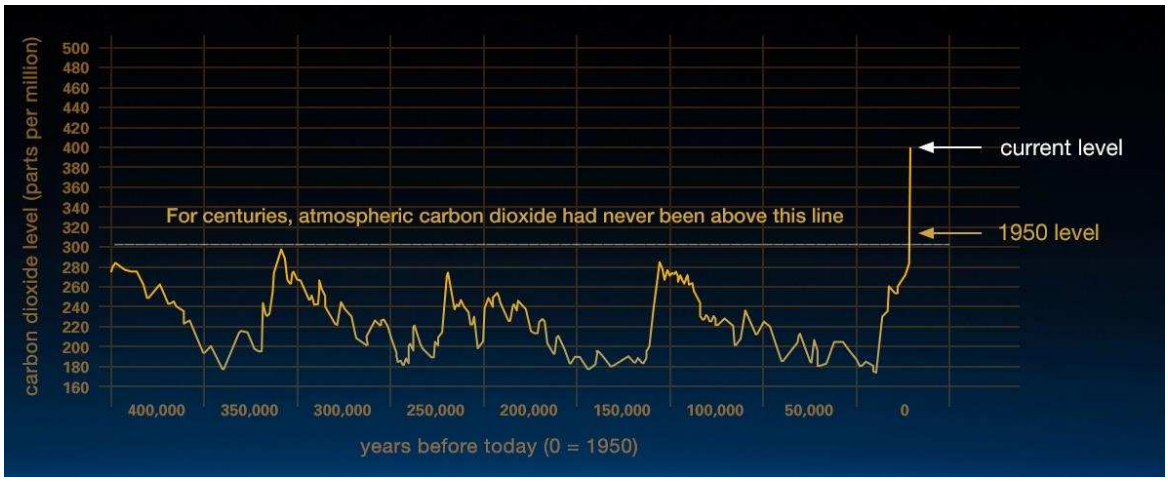

Figure 4: Historic global carbon dioxide levels (NASA, 2016)

In addition to greenhouse gases (GHGs), cookstoves also produce particulate matter (PM) emissions containing black carbon. Black carbon (BC) is most commonly known as "soot." BC is emitted from a wide range of combustion sources including wild fires, internal combustion engines, fossil fuel processing and combustion, and biomass stoves used for cooking and heating, and is generally a product of inefficient combustion. Greenhouse gases have a much longer lifetime in the atmosphere than black carbon and can last anywhere from decades to millennia which allows them to become more thoroughly mixed (United States Environmental Protection Agency, 2012). The extended lifetime (up to thousands of years, depending on how long it takes to make its way from the atmosphere into an ecosystem) of CO_2 is why it is the primary target

for emissions reduction; while in the atmosphere it continues to absorb energy. BC emissions are highly regional with short atmospheric lifetimes (Bond, et al., 2013). The short lifetime of BC in the atmosphere represents the potential for a short term mitigation strategy for reducing anthropogenic climate forcing.

1.1 OPPORTUNITY FOR REDUCING THE IMPACT OF COOKSTOVES BY USING AIR-INJECTION

Chimney cookstoves are used throughout the world and have a wide range of designs from residential home use to institutional settings where food is provided to hundreds of people. Forced air injection is a technological development that could show immediate benefits in terms of climate forcing. Additionally, the health implications are far reaching. With both indoor and outdoor air pollution being major health concerns, air injection technology could potentially decrease acute health effects such as COPD, IHD, and stroke that are caused by both indoor and outdoor air pollution. Air injection stoves use a fluid movement device, usually a fan, to force air into the combustion chamber of the stove. Previous work at the Advanced Biomass Combustion Laboratory (Dischino, 2015) tested a similar technology on low firepower (2.5-3.0 kW) rocket elbow stoves, and found significant reductions in PM emissions on two different stoves (Envirofit G3300 and M5000). The focus of this study is to understand the effects of forced air injection/EGR on PM emitted by an institutional chimney stove.

1.2 GLOBAL ALLIANCE FOR CLEAN COOKSTOVES PILOT INNOVATION FUND

In April 2015 a Pilot Innovation Fund (PIF) was awarded to the Advanced Biomass Combustion Laboratory at Colorado State University by the Global Alliance for Clean Cookstoves (GACC). This funding was used for several innovative technological developments, two of them being Exhaust Gas Recirculation (EGR) and ambient air injection in institutional

chimney stoves. These two technologies were developed, tested and compared to understand which of the two is more effective at particulate matter (PM) emissions reduction (Advanced Biomass Combustion Laboratory, Colorado State University, 2015). Elemental carbon (EC) and organic carbon (OC) emissions were also measured for both EGR and air injection systems. Between April 2015 and October 2016, the Advanced Biomass Combustion Laboratory has researched, designed, fabricated, and tested both EGR and air injection systems for the Envirofit EFI – 100L Institutional Cookstove, seen in Figure 5. High firepower cookstoves such as the Envirofit Institutional (15 kW), are used primarily in institutional settings such as schools. Although the EFI-100L Institutional Cookstove was used to evaluate air injection and EGR technologies, the developed technology could likely be applied to other stoves of similar size and design.

Figure 5: Envirofit EFI - 100L Institutional Cookstove

1.3 CARBONACEOUS AEROSOLS

In an effort to curb anthropogenic effects on the climate, the Kyoto Protocol targets GHG emissions from industrialized nations for reduction (United Nations, 2014). There has been a tremendous international effort put into identifying GHG sources, and implementing technology that limits GHG emissions. Targeting GHGs is a long term mitigation strategy. The short atmospheric lifetime of carbonaceous aerosols (BC and OC) makes them a prime target for a short term climate change mitigation strategy (Kopp & Mauzerall, 2010). An aerosol is a suspension of solid or liquid particles in a gas. Particles range in size from 0.002 – 100 μm (Hinds, 1999). Particles can be generated from a number of sources: dust, dirt, biological sources, and combustion. Chemically, BC is elemental carbon (EC) in a variety of structures (Kopp & Mauzerall, 2010). Soot aerosols absorb and scatter solar radiation (Ramanathan & Carmichael, 2008). High absorptivity of visible light distinguishes BC from other aerosols. In addition to having high absorptivity, BC also has low chemical reactivity in the atmosphere and is primarily removed by wet or dry deposition (Bond, et al., 2013). BC itself has a net-warming effect on the climate due to positive radiative forcing (RF) (Kopp & Mauzerall, 2010).

Black carbon mitigation efforts could prove difficult due to the fact that BC emissions are highly regional, which results in both net-cooling and net-warming effects (Bond, et al., 2013). For example, BC emissions from a region that is close in proximity to snow/ice cover could deposit on the snow/ice and decrease the surface albedo, which has a net-warming effect. After aging, BC emissions increase in size and hygroscopicity, which increase its cloud condensation nuclei potential (Bond, et al., 2013). An increase in cloud cover could result in net-negative climate forcing. BCs role in the atmosphere as a contributor to either net-warming or net-cooling is highly dependent on co-emitted particles/aerosols; BC rarely exists by itself. In addition to

BC, the combustion of biomass also produces organic carbon (OC) molecules, nitrates, sulfates, brown/yellow carbon, and gaseous constituents (United States Environmental Protection Agency, 2012). The overall effect of cookstove exhaust on global climate depends on the ratio of black (elemental) carbon to organic carbon.

Organic carbon (OC) generally refers to compounds containing carbon that are bound to other elements like hydrogen or oxygen. OC is either coemmitted with BC, or forms through oxidation of volatile organic compounds (VOCs) in the atmosphere (United States Environmental Protection Agency, 2012). Kopp et al. describe OC as generally having a net-cooling effect on the atmosphere whereas BC tends to usually have a net-warming effect. While OC generally tends to scatter radiation, there are also light absorbing species (Junker & Liousse, 2008). OC is very complex, and not as easily defined as EC. "Organic Carbon" refers to the carbon mass within organic aerosols (OA), excluding the oxygen and hydrogen content. The ratio between OA and OC (OA/OC ratio) depends on the amount of oxygen and other heteroatoms incorporated in the organic molecule (Bond, et al., 2013). The value of this ratio can range from 1.1 to 2.2 depending on the source, with coal and diesel having lower OA/OC ratios and biomass having higher OA/OC ratios (Russell, 2003). Using this ratio could help with determining the overall mass of what is referred to in this work as OC. However, determining the overall mass emitted by the stove is completed by gravimetric analysis. Organic carbon measurements refer to the carbon mass within OA's. It is acceptable for the purpose of this investigation to omit this factor from calculations which determine the OC fraction of exhaust because this investigation focuses primarily on the EC/OC and total PM.

To date there has been relatively little research on how biomass emissions affect the global climate. Kodros et al. go into great depth on these uncertainties (Kodros, et al., 2015).

Uncertainties in the effects of biomass emissions on the climate are partially due to the fact that biomass emissions are highly regional (Bond, et al., 2013). Uncertainties also result from the fact that interactions between BC and clouds are not yet well understood (United States Environmental Protection Agency, 2012). Despite the given uncertainties, it is generally accepted that reducing black/elemental carbon emissions, and overall particulate matter emissions is an important step towards reducing anthropogenic impacts on climate (Kopp & Mauzerall, 2010).

1.4 PARTICULATE MATTER (PM) AND THE WATER BOILING TEST (WBT)

The Global Alliance for Clean Cookstoves outlines a protocol for measuring a stove's performance. This protocol, the water boiling test (WBT) 4.2.3, is the result of many contributors. The tests measure the amount of pollutants emitted from the stove during a three phase test that is meant to replicate stove operation. The first phase is a cold start, which simulates cooking by starting the stove with a pot of water and operating at high firepower until the water boils. Phase two is a hot start, where a pot of water is boiled on a stove that is already at operating temperature. The final phase is a simmer test, where the water is kept at a boil for 45 minutes while operating at a firepower just enough to sustain a simmer. Emissions measured are carbon monoxide (CO), PM, and carbon dioxide (CO_2). Although CO and CO_2 are measured these results are not presented in this investigation; PM is the primary pollutant being analyzed.

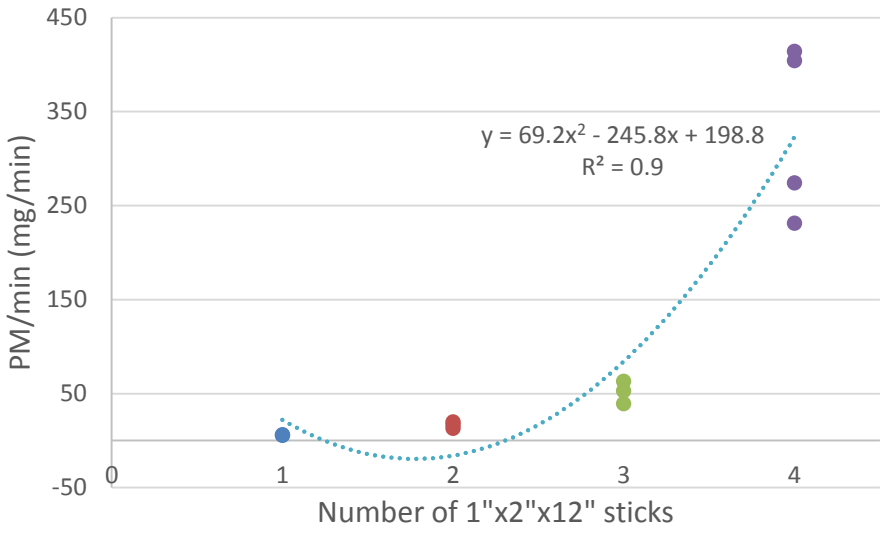

Figure 6: PM increases quadratically as fueling increases

Preliminary test results show that PM increases quadratically as fueling increases. Figure 6 shows the relationship between PM and fuel loading. During the cold start portion of the WBT the stove is being operated at high firepower, which produces the most PM relative to stove operation. For this reason, all tests performed throughout this study focus on the cold start portion of the WBT.

1.5 POTENTIAL FOR UNINTENDED CONSEQUENCES OF USING AIR-INJECTION

The results of this investigation and previous work are promising in terms of both climate impact and human health. Particulate matter and elemental carbon are prime targets for emissions reduction because of the almost immediate (in comparison to CO_2 reductions) benefit to climate change and the health concern they pose to human health, both indoor and outdoor. However, unintended consequences might result from the use of air injection and EGR as a means to reduce PM emissions. Recent research suggests that although PM is reduced by using forced air injection it increases the total ultrafine (less than 100nm in diameter) particle concentration (Rapp, Caubel, Wilson, & Gadgil, 2016). This is a major health concern because

fine/ultrafine particles are more dangerous than larger particles. Large particles (PM_{10}) are deposited primarily in the nose and throat due to their larger mass/inertia, but ultrafine particles ($PM_{0.1}$) are deposited deep in the lungs. Biomass cookstoves produce particle emissions with a lognormal distribution centered on 0.2 μm (L'Orange, Volckens, & DeFoort, 2012). Since biomass cookstoves produce more fine particles than coarse particles, their emissions are cause for concern. The deposition of fine/ultrafine particles into the lungs is dangerous for a few reasons: smaller particles are difficult for the body to remove and may remain in the lungs much longer than larger particles, so they have a greater biological effect than an equal mass of larger particles (Lighty, Veranth, & Sarofim, 2011). In addition to the health effects, smaller particles reduce visibility outdoors (EPA, 2016). Air injection has been shown to influence the particle size distribution of biomass cookstove emissions (Rapp, Caubel, Wilson, & Gadgil, 2016).

Rapp et al. suggest that with air injection, the particle size range with the largest PM generation rate is 5-100 nm; this was shown to be true with all of the stoves tested. Particles smaller than 2.5 μm are referred to as $PM_{2.5}$. The EPA has targeted fine particles for reduction due to the health and environmental implications (EPA, 2016). The most efficient air injection stove Rapp et al. tested produced the least total $PM_{2.5}$ mass, but generated more ultrafine particles (smaller than 30 nm) than the other stoves tested, including a three stove fire. It is important to note here that the stoves being tested are much smaller, lower firepower (5 kW) stoves than the Envirofit EFI – 100L Institutional (15 kW). Because they are not institutional chimney stoves, but rather residential rocket elbow stoves, they use air injection nozzles that are very different in design than the nozzles used in our tests. Also, they report to have measured an overall reduction in $PM_{2.5}$ mass of 35% and 66% for their Berkley Umbrella Stove (BUS) and Berkley Shower Stove (BSS) when compared to a three stove fire. While these reductions are

significant, 65% and 34% of the PM generated is still being emitted, respectively. In terms of total mass of PM emitted normalized to fuel consumed, the CSU Advanced Biomass Combustion Laboratory reduced PM emissions by over 90%. A significant decrease, such as 90% or more, in total PM emitted could prove beneficial to both the environment and human health despite the shift towards small particles. Although particle size could be shifted more toward ultrafine particles, extreme reductions in PM overall could also reduce the amount of ultrafine particles. This shift in particle size observed with the reduction of PM is an important consequence of using forced air injection, and warrants further investigation.

2 SYSTEM DEVELOPMENT AND LABORATORY TEST SETUP

In order to evaluate the effects of air injection on institutional cookstove emissions several different air injection manifolds, referred to as nozzles, were developed which interface with the combustion chamber of the stove. Section 2.1 discusses nozzle development for air injection, and section 2.2 discusses the EGR system development. These nozzles were designed such that they could be easily installed and removed, so that each nozzle could easily be tested on the same stove.

2.1 AIR-INJECTION MANIFOLD

A series of air-injection manifolds were designed, fabricated, and tested to find the best overall reduction in PM emissions from an Envirofit EFI – 100L Institutional cookstove. Two different styles of nozzles were fabricated. The first style was made from 3/8-inch Swagelok tubing, and the second was made of 304 stainless steel sheet metal. Each nozzle has either 5 or 16 orifices and different orifice diameters (2, 3, and 4 millimeters); see Table 1. Previous work (Dischino, 2015) shows that a circular nozzle with 12 1.5mm holes reduced PM emissions by 84% in a low firepower (3kW) cookstove. Dischino's work tested orifice diameters ranging from 1.5mm to 3.0mm. The previous success of Dischino's work led to the development of the 6 nozzles in Table 1, which have varying orifice diameters and numbers of orifices.

Table 1: Air Injection Nozzles

Nozzle	Orifices	Orifice diameter (mm)
5x2mm	5	2
5x3mm	5	3
5x4mm	5	4
16x2mm	16	2
16x3mm	16	3
16x4mm	16	4

2.1.1 SWAGELOK AIR INJECTION NOZZLE CONSTRUCTION

Swagelok tubing was originally used with the intent of simplicity. Rather than an elaborate assembly that requires a lot of tedious welding, a nozzle created from a single tube would only require a few operations: cutting the tube the correct length, rolling the tube into a circle, forming the inside of the circle so that it can be drilled, drilling the orifices evenly around the ring, and then welding a fitting onto the nozzle so it can be attached to the source of compressed air. The nozzle only requires two pieces of hardware; the tubing and the Swagelok fitting that is welded to the fitting. The simplicity of fewer parts is undermined by the fact that forming the tube into a ring such that each orifice can be drilled in the same orientation and evenly around the ring is extremely difficult to do by hand. For this reason, only two nozzles made from tubing were tested.

Figure 7: 16x3mm Swagelok air-injection nozzle

2.1.2 SHEET METAL AIR INJECTION NOZZLE CONSTRUCTION

Individual components were designed as parts of an assembly, then cut from a 4x8 foot sheet of 16 gauge (0.0625-inch) 304 stainless steel using a 3-axis waterjet. On site sheet metal fabrication tools were used to cut, roll, bend and otherwise form the sheet metal parts into the desired shape before they were welded together to finish the fabrication.

Figure 8: 5x2mm and 16x4mm air-injection nozzles (left and right, respectively)

Sheet metal nozzles are superior to the Swagelok nozzles for several reasons. Since they are designed in Solidworks as a sheet metal part, each nozzle is sure to be manufactured the same way with the only difference being the orifice size and number. Unit to unit variability was not tested in this investigation. Once the assembly was created in Solidworks, all that was changed to make each nozzle was the orifice diameter (2, 3, and 4mm), and number of orifices (5 and 16). The manufacturing process for these nozzles was much more consistent than using Swagelok tubing, and ensured far less variability in nozzle geometry.

2.1.3 AIR INJECTION OPERATION

Swagelok tubing was used to connect compressed air to an Alicat (Alicat Scientific, 2016) mass flow controller which was then connected to the air-injection nozzle. A 3/8-inch female Swagelok fitting was welded to each nozzle to make the connection between the nozzle

and the tubing. Preceding the nozzle is a 3/8-inch 304 stainless steel Swagelok tube that has been bent/formed to the stove such that it is easy to connect to, and out of the way of incoming fuel (Figure 9).

Figure 9: Swagelok tubing leading to air-injection nozzle

2.1.4 PLACEMENT

Nozzles were placed directly above the combustion chamber, at the bottom of the lower chimney section (Figure 10). This location was chosen based on previous research performed at the Advanced Biomass Combustion Laboratory at Colorado State University (Dischino, 2015) which showed substantial benefits to being located there. Flames exist in this region of the stove, which suggests that there is fuel left to be consumed. Injecting air here provides oxidizer in addition to what is entering through the mouth of the stove, and also thoroughly mixes the fuel and oxidizer. Each nozzle was placed in the same location seen in Figure 10.

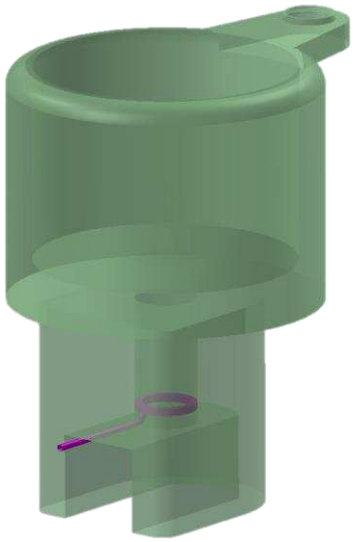

Figure 10: Air-injection location on Envirofit EFI - 100L Institutional cookstove

2.2 EXHAUST GAS RECIRCULATION (EGR)

Exhaust gas recirculation (EGR) is a method commonly used in internal combustion engines to reduce NO_x emissions (Hussain, Palaniradja, alagumurthi, & Maninaran, 2012). EGR recovers exhaust gas, and recirculates it back into the combustion chamber. EGR has previously been found to reduce emissions on rocket elbow stoves at the CSU Advanced Biomass Combustion Laboratory.

Figure 11: Prototype EGR system

The nozzle designed for the EGR system used the same geometry as the best performing (in terms of PM reduction) air-injection nozzle, the 5x2mm (Figure 12). However, the geometry of the nozzle could not be exactly the same due to the fact that the EGR system utilized a fan to provide the exhaust gas. With a fan, the pressure drop between the fan and the nozzle must be considered in the design so that the EGR system can provide adequate flow to the nozzle.

Figure 12: EGR injection nozzle

Figure 12 shows the nozzle before the fabrication was complete so that the fluid path can be better recognized. To keep the pressure drop between the fan and the nozzle as small as possible

the nozzle was designed to have nonrestrictive geometry. As can be seen in Figure 12, following the red arrows, exhaust gas enters the nozzle via a 4-inch inlet, and exits through 5, 2mm orifices.

Figure 13: EGR inlet, fan, and ducting connected to the cleaning port found directly below the chimney

Flexible 3.25-inch ducting was used to draw exhaust from a preexisting cleaning port directly below the chimney, and redirect it around towards the mouth of the stove. The cleaning port is normally used for cleaning the chimney. Near the front of the stove the 3.25-inch ducting was connected to two 4-inch elbows, and then the nozzle.

Figure 14: Left - 3.25-inch ducting that routes exhaust gas to the front of the stove; Right – 4-inch elbows between nozzle and 3.25-inch duct

All ducting connections were sealed with either high temperature silicone or high temperature insulation tape/gasket to ensure a leak-free system, as seen in Figure 14. After the EGR system was bolted into place and sealed it was ready to operate. Operating the EGR system was much different than operating the air injection setup.

2.2.1 EGR OPERATION

Operating the EGR system was challenging because it utilized a fan to recirculate the hot exhaust. The fan used was a custom built centrifugal fan designed specifically for this project; a pressure curve was not available for this fan. The motor is a brushless Turnigy D3536/8, and has a maximum power output of 430W. This motor requires a motor speed controller and a signal generator that measures the motor's speed in RPM. With all of these components properly connected, power was supplied at a constant 17.1V with a DC power supply, and the signal generator (tachometer) was used to control the speed of the motor.

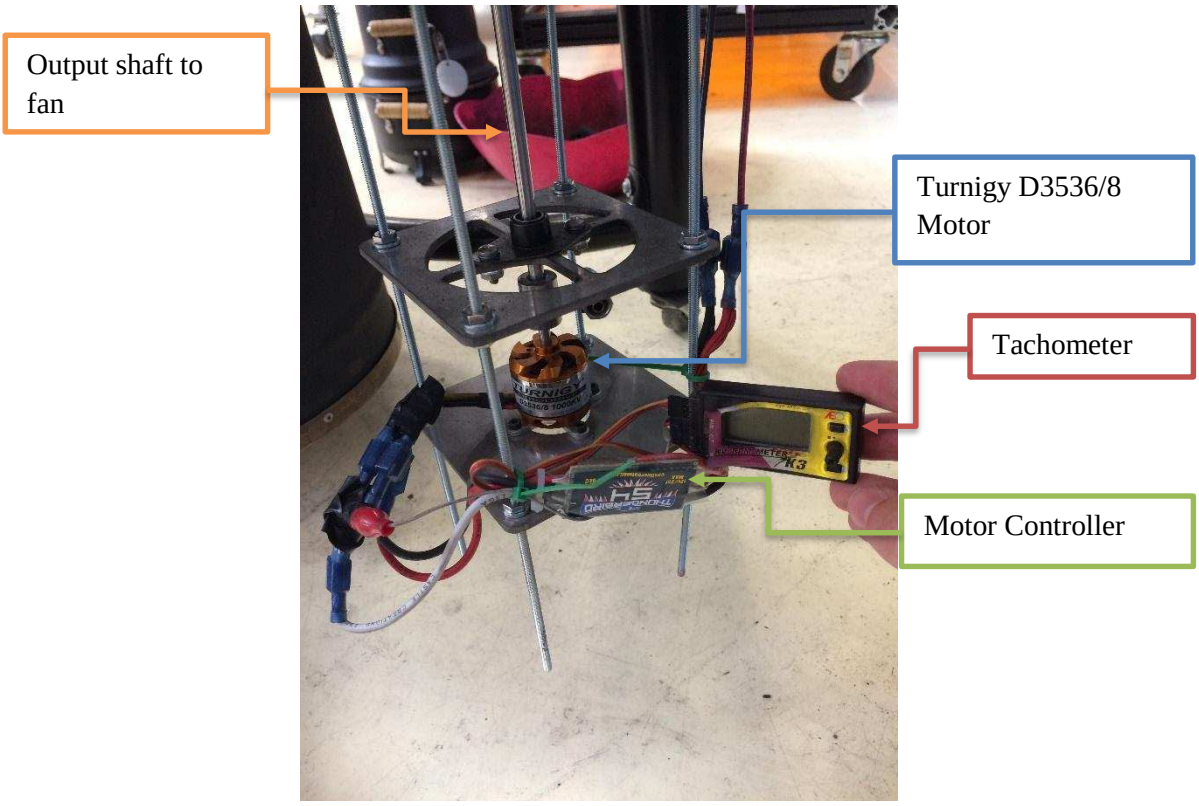

Figure 15: EGR fan motor, controller, RPM - Meter, and output shaft.

As stated previously, there is no pressure curve for this fan so it was difficult to know exactly what the flow provided by this fan is. To figure out the flow rate provided by this fan with this ducting and nozzle a 21.4-liter bag was repeatedly filled with air provided by the nozzle. Voltage was held constant at 17.1V, and the signal generator was used to change the fan's speed, and thus the flow through the nozzle. As can be seen in Figure 16, the maximum flowrate the fan is able to provide is approximately 48 LPM.

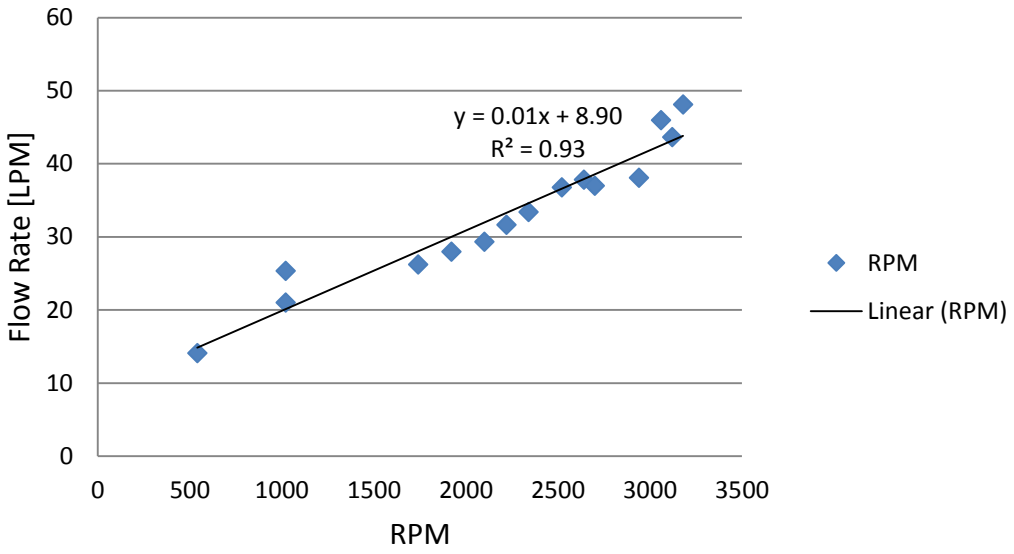

Figure 16: Volumetric flow rate vs. fan motor RPM

3 EMISSIONS TESTING

3.1 CYCLONE & FILTER SETUP

All samples drawn from the test hood are collected with an isokinetic probe. Figure 40 in the appendix shows a diagram of the test setup and the appropriate calculations to support isokinetic flow into the probe. The cyclone being used has a 2.5 μm cutpoint, and requires 16.7 liters per minute (LPM) of flow. Figure 17 shows the cyclone and filter housing.

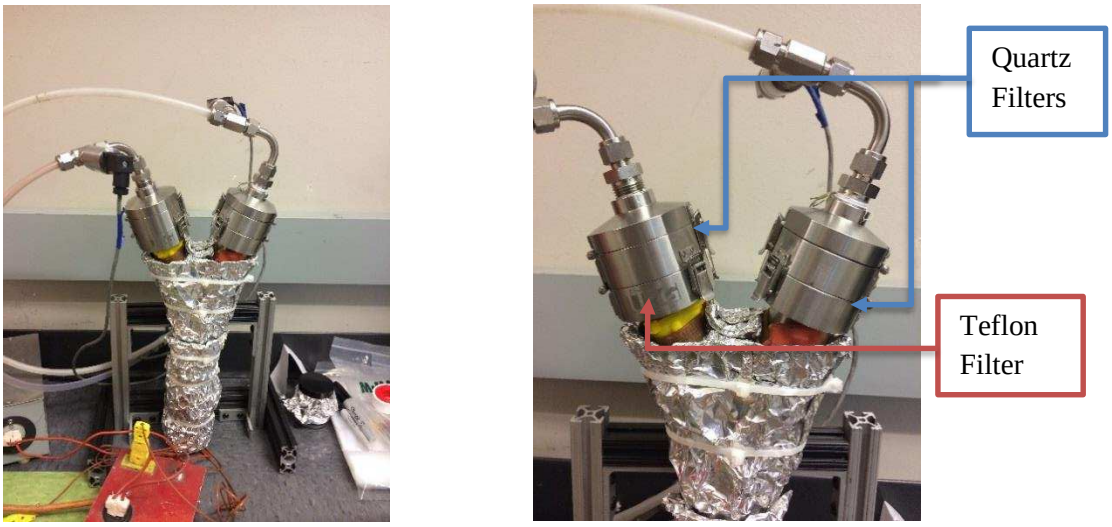

Figure 17: Cyclone and Filter Housing

The entire assembly can be seen in the left of Figure 17, and a close up of the filter housing on the right. It is necessary to keep the cyclone and filter housing warm to avoid water vapor condensation. This is achieved by wrapping everything upstream of the filter housing in heater tape that keeps it at a constant 46 °C. After being wrapped in heater tape, the assembly is wrapped in insulation and aluminum foil. A pressure transducer to measure filter pressure drop is installed downstream of each filter housing. A very large pressure drop across a filter is an indication that the required flow for the cyclone may not be achieved.

Two quartz filters, and one Teflon filter were needed to quantify EC and OC. The quartz filters are required to quantify the amount of solid phase EC and OC in both gas phase and solid phase. Filter placement can be seen in Figure 17. Since 16.7 LPM is required for the cyclone to work properly, this flow rate is split between each filter holder, so that each line pulls 8.35 LPM. Since the cyclone requires a specific volumetric flow rate to achieve the necessary inlet velocity, the flow controllers must be set to actual liters per minute (ALPM).

3.2 TEST MATRIX AND NOZZLE SELECTION

A series of tests were conducted to determine the nozzle with the most significant reductions in PM mass emitted from baseline. With the stove operating at high firepower, air injection rates were varied. Gravimetric filter samples were collected for three minutes at each operating point. After testing several of the nozzles, a general trend was recognized in how the flow rate, orifice diameter, and orifice number affect PM emissions.

Table 2: Air-injection flow rate test matrix

5x2mm		5x3mm		5x4mm	
Flow Rate	PM/min	Flow Rate	PM/min	Flow Rate	PM/min
0 SLPM	183.9	0 SLPM	221.8	0 SLPM	53.1
20 SLPM	100.0	20 SLPM	61.1	20 SLPM	82.2
40 SLPM	41.9	40 SLPM	150.2	40 SLPM	100.0
60 SLPM	5.4	60 SLPM	97.3	60 SLPM	91.4
80 SLPM	15.3	80 SLPM	38.7	80 SLPM	31.1
100 SLPM	25.3	100 SLPM	12.8	100 SLPM	13.8
120 SLPM	51.6	120 SLPM	14.0	120 SLPM	39.6
140 SLPM	75.3	140 SLPM	18.5	140 SLPM	14.1
160 SLPM	101.9	160 SLPM	17.6	160 SLPM	17.4
16x2mm		**16x3mm**		**16x4mm**	
Flow Rate	PM/min	Flow Rate	PM/min	Flow Rate	PM/min
0 SLPM	89.8	0 SLPM	181.9	20 SLPM	79.7
20 SLPM	125.2	20 SLPM	92.8	40 SLPM	82.6
40 SLPM	132.8	40 SLPM	78.0	60 SLPM	107.2
60 SLPM	63.3	60 SLPM	24.6	80 SLPM	160.8
80 SLPM	23.0	80 SLPM	105.1	100 SLPM	153.6
100 SLPM	13.4	100 SLPM	17.5	120 SLPM	115.6
120 SLPM	11.3	120 SLPM	10.2	140 SLPM	159.5
140 SLPM	18.7	140 SLPM	12.9	180 SLPM	110.8
160 SLPM	22.3	160 SLPM	13.7		

Nozzles with fewer and smaller holes resulted in greater PM reductions. Figure 18 and Figure 19 show the PM reductions for each of the nozzles in Table 2. There is a clear trend in

PM reduction vs. flow rate. With the exception of the 16x4mm nozzle (Figure 19), every nozzle rapidly reduces PM as the flow rate increases, and then PM levels gently rise with flow rate after peak PM reductions are made.

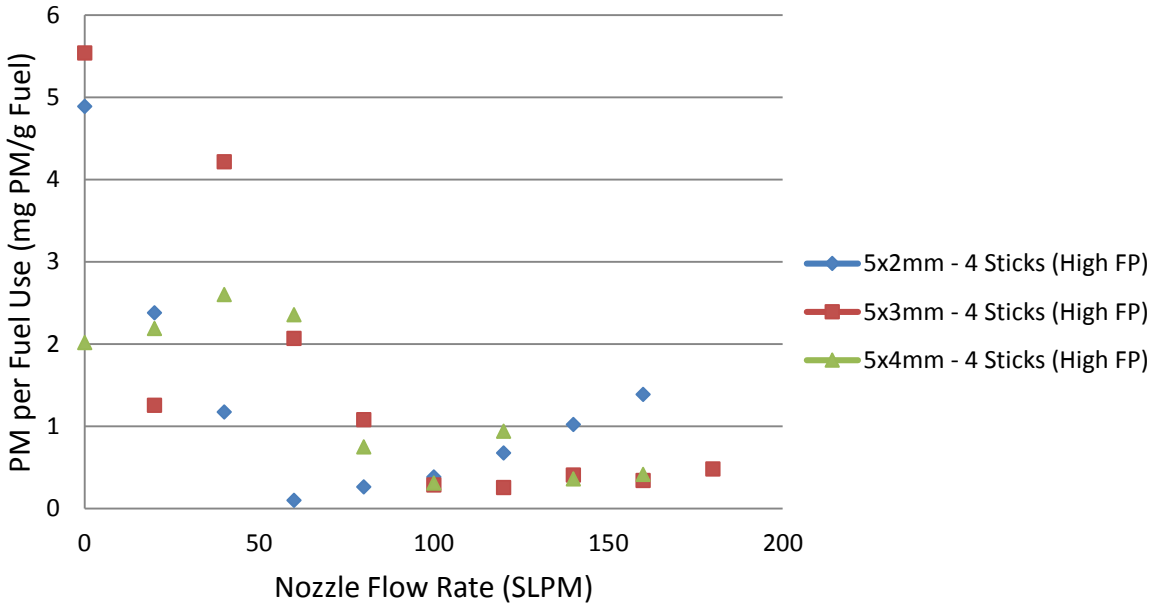

Figure 18: PM reductions with 5 orifice nozzles

Figure 18 and Figure 19 also reveal maximum PM occurs at different flow rates for each nozzle. The 5 orifice nozzles achieve their best PM reductions at lower flow rates than the 16 orifice nozzles. However, there are similar reductions in PM across several of the nozzles. Significant PM reductions are being made where the velocity of air exiting the nozzle is high and the mass of air is low (Ex.: 5x2mm nozzle at 60 SLPM), and also where the velocity of air exiting the nozzle is low and the mass of air is high (Ex.: 16x3mm nozzle at 120 SLPM). This leads to the hypothesis that PM reduction is driven by increasing access to oxidizer. There appears to be two paths to increasing access to oxidizer: increased mixing and turbulence due to high velocity jets and increased total oxidizer. For example, similar PM reductions were seen between the 5x2mm nozzle at 60 SLPM and the 16x3mm nozzle at 120 SLPM. The injection

velocities were approximately 144 m/s and 43 m/s for these two nozzles, respectively. At this point in the experiments the nozzles with the best PM reductions were identified as the5x2mm and the 16x3mm.

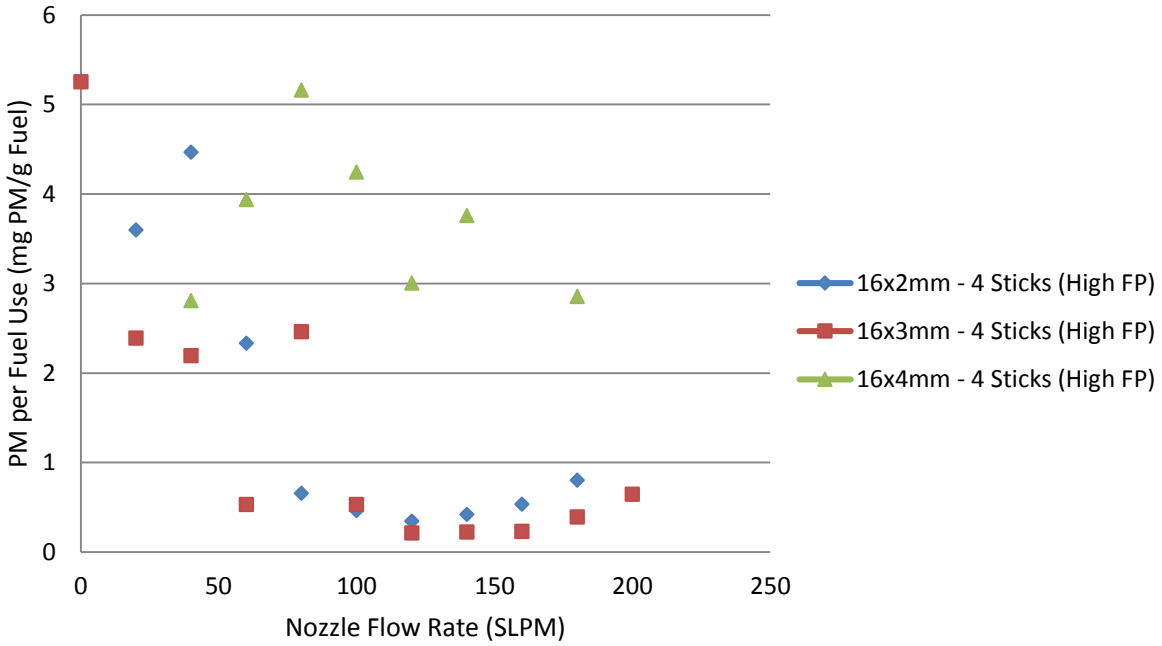

Figure 19: PM Reductions with 16 orifice nozzles

3.3 TOTAL FLOW THROUGH THE STOVE

Understanding the bulk flow through the stove is important for understanding where oxidizer is coming from. When a stove operates without air injection oxidizer is provided to the combustion chamber by air that is drafted in through the mouth of the stove. Without testing total bulk flow, it is unclear how oxidizer is reaching the combustion chamber. Air injection could be increasing total bulk flow, or it could be diverting flow from the mouth of the stove. Table 3 shows the total flow of air through the stove was measured for three different nozzle flow rates: 0 SLPM, 60 SLPM, and 100 SLPM. Total flow didn't change much with 60 SLPM of air injection.

To calculate the flow through the stove combustion is assumed to be stoichiometric. O_2 is measured in the chimney, and CO_2 and CO are measured by the 5-gas analyzer in the test hood. These measurements are taken at a frequency of 1 Hertz, so the mass flow rate of each can be calculated (kg/s). Excess air is calculated similar to the method above. Total flow is then calculated by adding stoichiometric air and excess air together. Figure 39 in the appendix outlines the equations used for these calculations in detail.

Table 3: Flow of air through the stove for 0, 60, and 100 SLPM

Nozzle SLPM	0	60	100
Average LPM Flow through stove	411	405	441

Flow through the stove is dependent on firepower. Firepower increases when fuel is added to the combustion chamber. Flow through the stove changes little with 60 SLPM, which means some flow is being diverted away from the mouth of the stove. With 100 SLPM of air injection the total bulk flow increases slightly.

3.4 TIMING AND FUELING

In the way of timing and fueling, test methods vary significantly for cold start tests and EC/OC tests. Cold start tests were performed according to the GACC WBT protocol 4.2.3 (Global Alliance for Clean Cookstoves, 2014). EC/OC tests were completed in the time it took to burn approximately 550g of fuel in total; this was usually between 10-15 minutes. The same fuel was used for both cold starts and EC/OC tests with the only difference being that the nominal size of the fuel was 1x2x12-inch and 1x2x6-inch, respectively. The size of the fuel was cut in half for EC/OC tests due to the fact that sometimes fugitive emissions were exiting the stove through the mouth rather than being drawn through the stove by buoyancy when 12” fuel pieces were used. To establish best case effects of air injection on the EC/OC ratio it is

necessary to ensure that all of the combustion products are drawn up through the stove. When fugitive emissions exit the stove through the mouth they are not treated by the air injection, and thus bias the data such that it does not represent the effects of the air injection. There are two possible reasons that fugitive emissions were exiting the stove through the mouth: With 12" pieces of fuel, the fire creeps down the length of the fuel, and combustion products are no longer buoyantly driven through the stove, but into the ambient environment. Second, fugitive emissions were worse with 16 orifice nozzles. With increasing orifices, the air being injected results in a sheet of air that impedes the draft of the stove. Cold start tests completed on 16 orifice nozzles with 1"x2"x12" fuel observationally had worse fugitive emissions than the 5 orifice nozzle cold start tests.

Starting material, referred to as "shim packs," can be seen in Figure 23. Three or four of these shim packs were used to start the stove, depending on weight. Shim packs were used for each cold start and EC/OC test. The moisture content of fuel was measured to be approximately 6% for each test.

3.5 COLD START/EGR TESTS

The Envirofit EFI – 100L Institutional cookstove creates a high amount of PM during start-up. Since the goal of this project was to better understand the use of air injection and EGR as an emissions reduction technology the focus of testing was kept to the cold start portion of the WBT (Global Alliance for Clean Cookstoves, 2014). This phase of the WBT characterizes the stoves performance between start-up and when the water is boiling. For the Envirofit EFI – 100L Institutional, this is the most critical test phase. It is a very large, high firepower stove, so it takes much longer than smaller stoves that use the same testing protocols and it creates a high

amount of PM in the process of boiling water. WBT 4.2.3 was followed for each cold start test performed on both air injection and EGR.

Figure 20: Envirofit EFI - 100L Institutional cookstove in the test hood with air injection during a cold start test

Figure 20 shows the Envirofit EFI – 100L Institutional cookstove in the test hood with an air injection nozzle installed during a cold start test. To prepare for the test:

- Exactly 75 liters of 15°C water is added to the pot
- A large quantity (roughly 3500 g) of fuel (1”x2”x12” pine furring strips) is weighed
  - Starting material is weighed separately
- A gravimetric filter is placed in the filter holder
- The stove is then placed in the test hood
  - Water temperature thermocouple is placed in the pot
  - Chimney temperature thermocouples are placed at the base of the chimney
- All necessary computer software/data acquisition tools are turned on and prepared for testing

- Air injection/EGR flow rate are set to the desired value and left for the remainder of the test
    - High air injection flow rates sometimes required ramping

When all of the above steps have been taken to prepare for the test the gravimetric pumps are turned on, mass flow controllers are set to the required flow rate, and the starting fuel is lit with a propane torch. The starting material is placed in the stove and allowed to burn until there is enough of a fire to begin adding fuel. Starting material generally burns fairly quickly, so fuel can be added almost immediately. For some of the air injection tests the flow rate was ramped so that the starting fuel was not extinguished. For example, if the air injection flow rate being tested is 120 SLPM, the starting material could be extinguished due to its close proximity to the high velocity air exiting the nozzle. So, the air injection may start at 60 SLPM so that the starting material burns well enough to begin adding fuel, and then ramp to 120 SLPM in increments of 30 SLPM. This process usually took less than 5 minutes. Air injection flow rate was only ramped if it was clear, observationally, that ramping was necessary. If the fire was completely extinguished, or if the starting material was having trouble staying lit the flow rate was decreased and then ramped. If the starting material is blown out by the nozzle the flow rate is reduced so that the fire can be started, and then ramped appropriately.

During the test, 4 pieces of fuel are continuously fed into the combustion chamber using the fuel spacer. Fuel is continuously fed into the stove until the water is boiling, at which point the mass flow controllers are set to 0 SLPM. At this point the test is over, and the gravimetric filter can be collected from the filter holder for post processing.

Only one cold start test was performed on the EGR system. This system performed so poorly that it did not warrant further testing. The EGR fan was set to its highest flow rate

(approximately 48 ALPM) and kept constant through the test. During the test, fugitive emissions were exiting the stove through the mouth rather than drafting properly and exiting through the chimney. The fugitive emissions were so severe that, observationally, almost no exhaust was being drafted through the stove. This is an indication that the draft of the stove is being collapsed.

3.6 EC/OC TESTS

Testing the EC/OC content from the Envirofit EFI – 100L proved to be fairly difficult. Baseline tests conducted in July 2015 collected so much particulate matter that it began to delaminate from the filter. For this reason, EC/OC tests conducted for air-injection were much shorter than the baseline (cold start) tests. For each flow rate, 93g ± 9.7g of starting material was weighed, and 462g ± 13.8g of fuel. Variation in these numbers between tests due to the nonuniformity of the fuel itself. There are three replicates of each flow rate for each nozzle (see Table 4).

Table 4: Air-Injection EC/OC Test Matrix

	30 SLPM	60 SLPM	90 SLPM	120 SLPM
5x2mm	3	3	3	3
5x3mm	3	3	3	3
16x3mm	3	3	3	3

The flow rates in Table 3 were chosen so that the best coverage of flow rates and injection velocities could be achieved, and so that a relationship between EC/OC ratio and flow rate could be identified. The nozzles were selected based on the exit velocity of air from the

nozzle at different flow rates. Figure 21 & Figure 22 show the exit velocity of air at each flow rate measured in ALPM and SLPM, respectively.

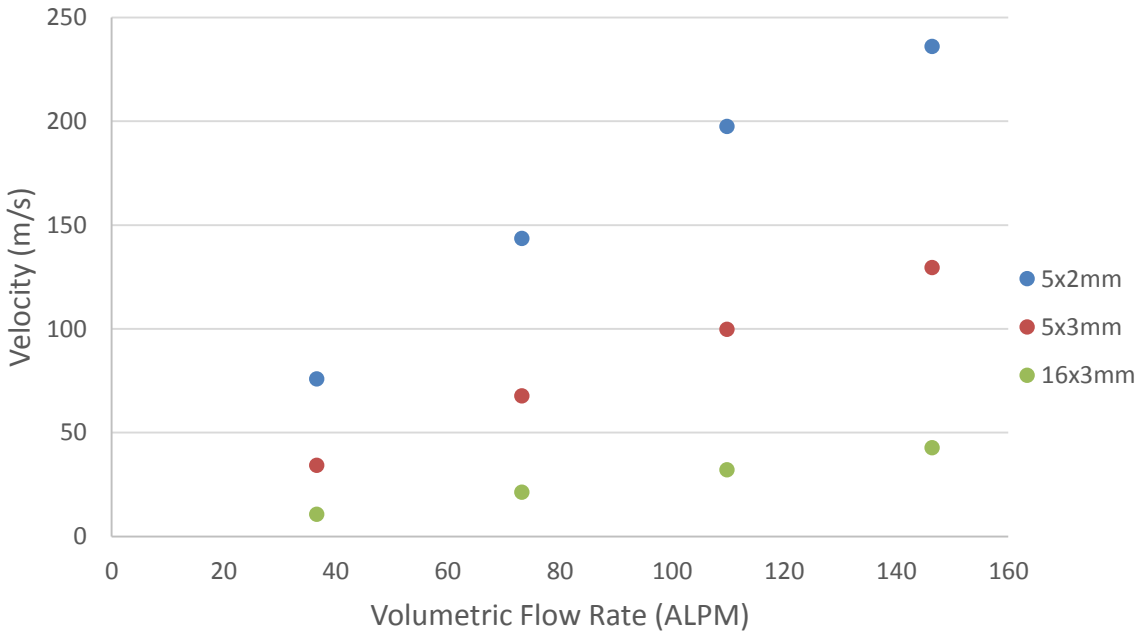

Figure 21: Velocity vs. Volumetric Flow Rate

Nozzles and air injection flow rates selected for EC/OC testing, which are highlighted in Figure 21 and Figure 22, cover the majority of velocities that are possible with the 6 original nozzles. The flow rate was limited to 120 SLPM so that fuel being lofted and exiting the mouth of the stove was not a problem during testing. To completely cover the possible range of velocities, the 16x4mm nozzle would have been chosen instead of the 16x3mm. The 16x3mm has the same geometry/fabrication method as the 5x2mm, and 5x3mm nozzles (sheet metal nozzles, 2.1.2) whereas the 16x4mm nozzle was made of Swagelok tubing (Swagelok air injection nozzle construction, 2.1.1). Additionally, the 16x3mm nozzle was chosen for a field prototype that was tested in Kenya over the month of August, 2016 (Prototype Air Injection System, 4.3). The difference in the velocities provided by the 16x3mm and 16x4mm nozzles are small in comparison to the overall range of velocities. Air injection was controlled in SLPM

rather than ALPM for all tests. Using SLPM is preferable to ALPM because the flow of air to the nozzle is measured with standard temperature and pressure, 25˚C and 14.696 psi respectively. This allows for consistent flow rates between tests. Using ALPM would result in different mass flow rates for every tests, depending on current local temperature and pressure. This is a meaningful difference during testing.

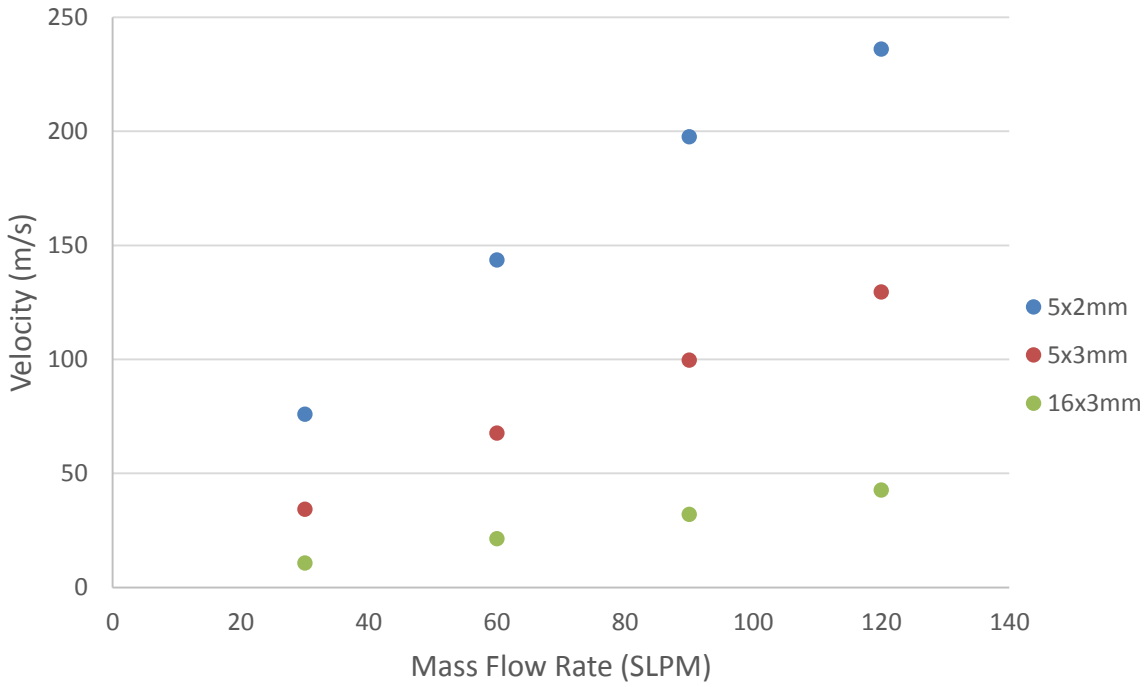

Figure 22: Velocity vs. Mass Flow Rate

Test details can be found in the appendix. For EC/OC test 6-inch pieces of fuel were used, and 3 or 4 shim packs were used (depending on weight) for starting material (Figure 23). Prior to beginning data collection, the stove was brought to operating temperature. Hot water (approximately 55-60°C) was added to the pot in the amount of 75 liters. This reduced the start-up time for the stove. The stove was then started, and the water brought to a boil as quickly as possible. Bringing the water to a boil helps ensure that heat transfer to the pot of water is constant, and the stove itself is at operating temperature.

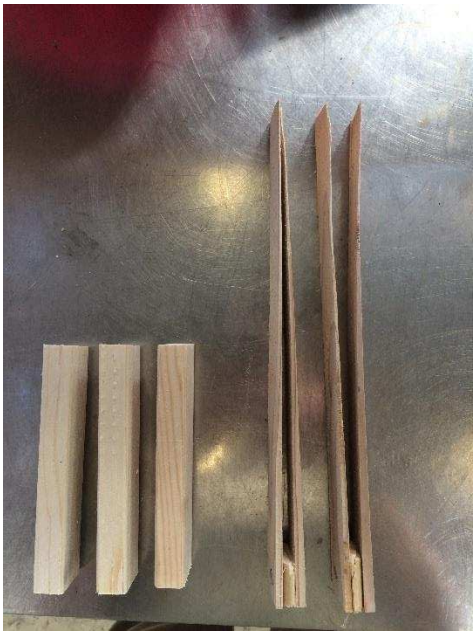

Figure 23: 6-inch fuel (left), starting "shim pack" material (right)

To begin the test, the shim packs were lit and placed in the stove. As soon as the shim packs are burning, the gravimetric pumps are turned on, and the stove's exhaust is being sampled. Fuel was then placed on top of the shim packs so that it would catch fire as quickly as possible. Combustion temperatures are very low during startup, which results in a high amount of PM being emitted. For that reason, it is essential to capture this phase of the stove's operation for each flow rate tested. Fuel is continuously added in increments of 1-2 pieces as the fire grows. Each time a piece of fuel is added the combustion temperatures drop slightly and then recover. The duration of the test must be long enough to capture the startup phase, several fuel additions, and then burnout. Burnout occurs after all of the fuel has been fed into the fire, and the fire consists of mostly, if not all, char. If CO is being measured during the test, burnout can be recognized when the amount of CO emitted/measured begins to rapidly rise. At this point, the gravimetric pumps are turned off, and the char is removed from the stove to be weighed. The filters are removed from the filter holder, and placed in petri dishes, then stored in a freezer for analyses.

3.6.1 EC/OC VOLUMETRIC FLOW

A sampling error was identified part way through the study. To account for this, the total amount of air that passed through each filter housing was calculated by numerically integrating the volumetric flow rate over the length of the test. Figure 24 shows an example of the flow rates over the duration of a test with a flow controller incorrectly set to SLPM.

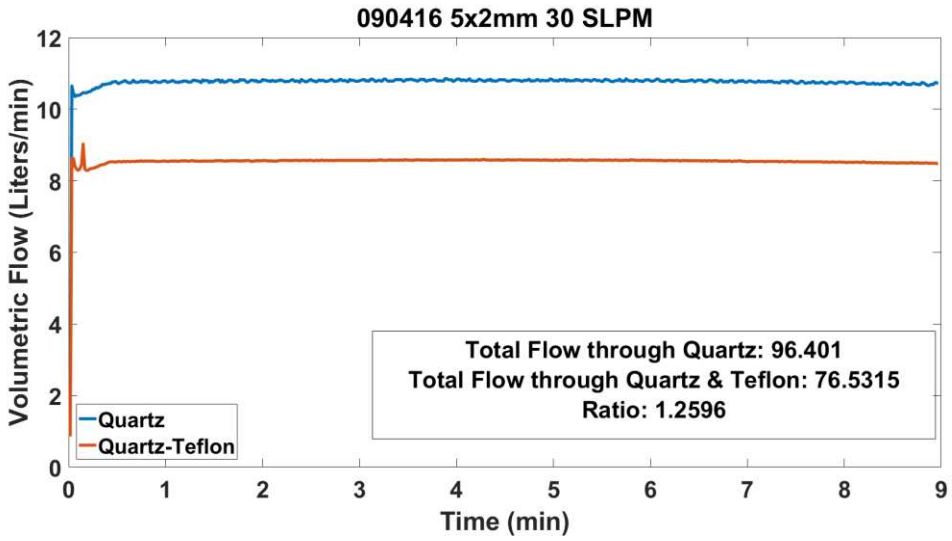

Figure 24: Example of volumetric flow rates through each filter holder

At the beginning of the test the flow controllers quickly adjust to the flow rate input. After that, the flow controllers maintain a nearly constant flow rate. The ratio of flow between the filter holders was calculated using the total volume of air passed through each filter holder. To continue the example from Figure 9, the total flow for that particular test was 96.4 L for the quartz filter holder, and 76.5 L for the quartz/Teflon filter holder. So, the ratio of flow between the two is 96.4/76.5 = 1.26. This ratio is used in both PM and EC/OC data to correct tests completed with a flow ratio not equal to one. Tests with both Alicat mass flow controllers correctly set to 8.35 LPM are assumed to have a flow ratio equal to one.

Table 5: Flow Ratios for Tests with Unequal Mass Flow Controller Settings

Nozzle, Flow Rate (SLPM), replicate	Flow Ratio (Quartz/Quartz-Teflon)
5x2mm, 30	1.26
5x2mm, 30, two	1.18
5x2mm, 30, three	1.18
5x2mm, 60	1.26
5x2mm, 60, two	1.26
5x2mm, 60, three	1.26
5x2mm, 90	1.26
5x2mm, 90, two	1.18
5x2mm, 90, three	1.18
5x2mm, 120	1.26
5x2mm, 120, two	1.26
5x2mm, 120, three	1.26
5x3mm, 30	1.17
5x3mm, 60	1.18
5x3mm, 60, two	1.17
5x3mm, 60, three	1.18
5x3mm, 90	1.17

3.6.2 ANISOKINETIC SAMPLING

With the flow ratios found in Table 5 comes the concern of *anisokinetic sampling*. Anisokinetic sampling can result in a biased estimate of concentration. Since one of the mass

flow controllers was incorrectly set to SLPM rather than LPM, the sampling probe inlet velocity is greater than the exhaust flow velocity in the duct; it is *superisokinetic*. Superisokinetic flow can result in underestimation of concentration because particles with high inertia cannot follow the converging streamlines to enter the probe, and are lost from the sample (Hinds, 1999). The tests completed under superisokinetic sampling conditions can be validated by calculating the Stokes number and the concentration ratio. The concentration ratio describes the ratio between particles entering the probe and particles in the free stream (duct).

$$Stk = \frac{\tau U_0}{D_s}$$

Equation 1: Stokes number (Hinds, 1999)

Here, U_0 is the free stream velocity, D_s is inside diameter of the sampling probe, and τ is the relaxation time of the particle. This is the time it takes for a particle to adjust to a new velocity. Details on these terms can be found in the appendix.

$$\frac{C}{C_0} = 1 + (\frac{U_0}{U} - 1)(1 - \frac{1}{1 + (2 + 0.62\,U/U_0)Stk})$$

Equation 2: Concentration Ratio (Hinds, 1999)

Equation 1 and Equation 2 were calculated to be 5.48×10^{-4} and 0.9998, respectively. This means that although the sampling was superisokinetic the concentration in the sampling probe was the same as the free-stream/duct. This is due in large part to the fact that biomass particles are very small, having a lognormal distribution centered on 0.2 μm (L'Orange, Volckens, & DeFoort, 2012). With a Stokes number so close to zero, and a concentration ratio of nearly 1 it is safe to include and compare the results of tests completed with superisokinetic sampling.

3.7 GRAVIMETRIC ANALYSIS

The CSU Advanced Biomass Combustion laboratory follows the same procedure for all gravimetric analysis (L'Orange, Standard Operating Procedure - Gravimetric Filter Handling, 2015). This procedure was the same for both cold start and EC/OC test filters. A brief explanation of the gravimetric analysis is as follows:

- Filter Handling
  - Filters are equilibrated to the microbalance laboratory air for 24 hours before being pre-weighed.
  - After being pre-weighed the filters are ready for testing, with necessary precautions taken during transport to avoid any mass accumulation on the filter.
  - Filters are placed in the filter holder (Figure 25) for testing.
  - After testing, the filter is removed and transported back to the microbalance laboratory, again with the necessary precautions taken to avoid any mass accumulation.
  - Filters are allowed 24 hours to equilibrate with the microbalance laboratory air, and then post-weighed.
- For each day that a test is conducted, a background PM sample is collected.
- The standard deviation (s) of test blanks are used to determine the Limit of Detection (LOD) and Limit of Quantification (LOQ) for gravimetric analysis.
  - Collection mass from Envirofit Institutional EFI – 100L is substantially greater than the LOQ.
  - $LOD = \Delta mass_{filter} + 3s = 9\mu g$
  - $LOQ = \Delta mass_{filter} + 10s = 25\mu g$

The quantification of gravimetric analysis results varies between the cold start tests and the EC/OC tests: cold start tests use a single sampling line whereas EC/OC testing uses two sampling lines. The analysis method is the same, but the mathematics used for quantification are slightly different between the two. This is due to the fact that the sample line is split during EC/OC testing. Referring to the left side of Figure 25, only one side of the flow splitter is used for cold start tests; all of the flow (16.7LPM) goes through a single filter. In the same figure on the right side it can be seen that both sides of the splitter are used for EC/OC tests; here the flow is split equally between the sides (8.35 LPM each).

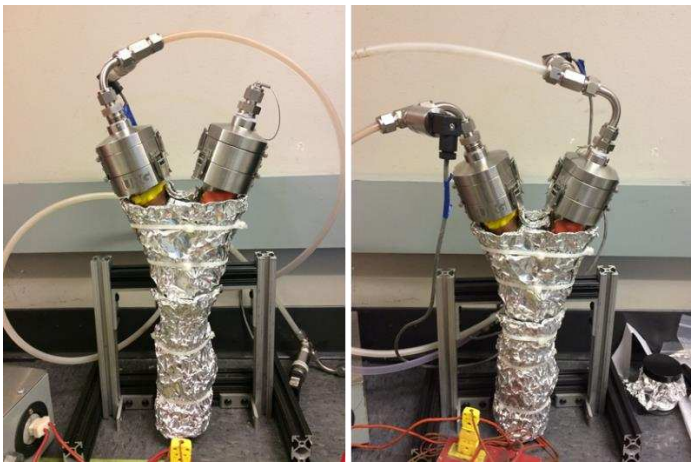

Figure 25: Left - Cold start test cyclone setup, Right - EC/OC test cyclone setup

The PM samples collected are a small fraction of the total stove emissions, and must be multiplied by 359.9 to determine the total PM emitted. This accounts for the fraction of flow captured by the filter; a diagram of the system and the necessary calculations can be found in the appendix, Figure 40. The total amount of PM emitted during a cold start test is the net mass collected on the filter minus the expected background PM multiplied by 359.9, see Figure 40. This value is in units of microgram (μg), and can be converted as necessary.

$$PM_{total,cold\ start} = (\Delta m_{filter} - \frac{\Delta m_{BG}}{time_{BG}} \times time_{test}) \times \frac{Q_{hood}}{Q_{probe}}$$

Equation 3: Total cold start PM

The total amount of PM emitted during an EC/OC test is not calculated this way because the flow is split between two filter holders, and only a single Teflon PM filter is used. Filter placement can be seen in Figure 17. The net mass on the Teflon filter is multiplied by 2 to account for the side that only has a quartz filter. This is, of course, assuming that the flow between the two sides is equal. However, as discussed in 3.6.1, nearly half the EC/OC tests were completed with unequal flow between the two sides of the splitter. To account for this, the ratio discussed in 3.6.1 was used to correct for the unequal flow.

$$PM_{total,\frac{EC}{OC},equal\ flow} = 2 \times (\Delta m_{filter} - \frac{\Delta m_{BG}}{time_{BG}} \times time_{test}) \times \frac{Q_{hood}}{Q_{probe}} \times \frac{1[mg]}{1000[\mu g]}$$

Equation 4: Total EC/OC PM with equal flow

$$PM_{total,\frac{EC}{OC},unequal\ flow} = \left(1 + \frac{Q_{Quartz}}{Q_{Quartz-Teflon}}\right) \times (\Delta m_{filter} - \frac{\Delta m_{BG}}{time_{BG}} \times time_{test}) \times \frac{Q_{hood}}{Q_{probe}} \times \frac{1[mg]}{1000[\mu g]}$$

Equation 5:Total EC/OC PM with unequal flow

Once the total amount of PM has been calculated it can be normalized to the amount of fuel consumed over the length of the test, resulting in units of $\frac{mgPM}{kgFuel}$. This allows for a direct comparison between tests, which is important for comparing the baseline (cold start) test results to the EC/OC test results.

3.8 EC/OC ANALYSIS

EC/OC samples were collected using the same cyclone and filter holder as the PM samples, but with a slightly different filter set up. Figure 25 shows the filter positions for both quartz and Teflon filters used during EC/OC tests. Three filters must be used so that only solid phase organics are accounted for rather than solid and gas phase. If only a single (quartz) filter were used it would include both solid and gas phase. Instead, there is a quartz filter which catches both solid and gas phase (labeled A, Figure 26) with half of the total flow passing through it, and a quartz filter preceded by a Teflon filter (labeled B, Figure 26) with half of the total flow passing through it.

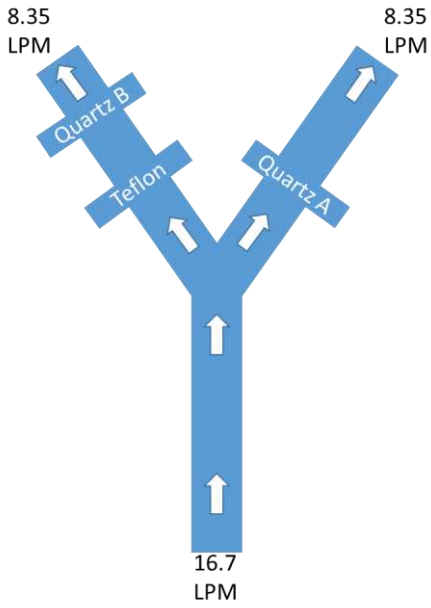

Figure 26: EC/OC filter setup

As mentioned in 3.6.1, the flow between sides A and B were different for some of the tests; this was accounted for by using a flow ratio to normalize the data. To do this, both EC and OC values for filter A were divided by their respective ratio. By dividing A by the ratio, it is then equal to B (Equation 6 and Equation 7).

$$m_{in} = m_A + m_B$$

Equation 6: Mass in equals mass collected on filters A and B

$$\frac{m_A}{m_B} = R$$

Equation 7: Flow Ratio

Total EC and OC were then calculated by subtracting B from A, which provides the total solid phase values. These totals were then normalized to the amount of fuel consumed, the flow ratio between the duct and probe, and converted from *μg* to *mg* providing units of $\frac{mg}{kgFuel}$.

$$Total = \frac{m_A - m_B - \left(\frac{m_{BG}}{time_{BG}} \times time_{test}\right)}{m_{fuel}} \times \frac{Q_{duct}}{Q_{probe}} \times \frac{1[mg]}{1000[\mu g]}$$

Equation 8: Total EC or OC

Units of $\frac{mg}{kgFuel}$ not only allow one to calculate the EC/OC ratio, but also allow for comparing the EC and OC values to the total PM emitted from the stove. While the EC/OC ratio is valuable, it is also interesting to see how forced air injection effects EC and OC as a percent of the total PM emitted. These results are discussed in 4.2.

In addition to collecting gas phase OC, both quartz filters collect some portion of volatile organic compounds (VOCs) emitted from the cookstove. The adsorption of VOC's onto the quartz filters gives a positive OC artifact (Fitz, 2007). Since the flow through each filter holder is equal, the amount of VOCs adsorbed to each quartz filter is also assumed to be equal. The adsorption of VOCs onto the quartz filters is assumed to be represented by the OC collected.

4 RESULTS AND CONCLUSIONS

4.1 EFFECTS OF AIR INJECTION ON PM

Error bars on all plots are a single standard deviation, and results tables provide both standard deviation and 80% confidence intervals for the given data. A confidence interval allows one to say that the mean of a population lies between two values, with a certain level of confidence (Navidi, 2011). While most scientific experimentation uses a 95% or 99% confidence interval, stove testing is inherently very variable. Using an 80% confidence interval is more realistic because of this inherent variability. Because of the small sample size, a t-distribution was used to calculate confidence intervals. To describe the final results of the PM testing a t-test with a significance level of 5% assuming unequal variance was used to show that the population means are different.

As discussed in 3.2, several nozzles were tested over a range of flow rates to determine the optimal air injection flow rate. Results from those tests (Figure 18 and Figure 19) indicate that nozzles with fewer and smaller orifices are more effective at reducing PM. The 5x2mm nozzle operating at 60 SLPM was the most effective at reducing PM compared to the other nozzles tested during the flow rate sweeps. Further testing focused on this nozzle and flow rate; several cold start tests were conducted to compare the overall high firepower PM reduction to the baseline test results.

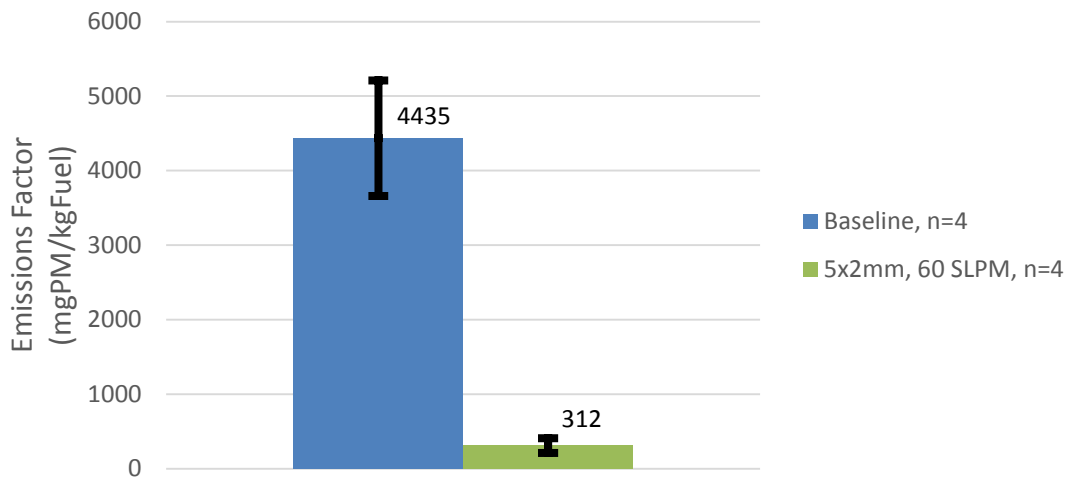

Figure 27: Emissions Factors comparison between baseline and best performing nozzle/flow-rate combination

As can be seen in Figure 27, there is a dramatic reduction in PM emissions with the use of air injection. The 5x2mm nozzle operating at 60 SLPM resulted in a decrease of 92% in total PM emitted from the stove. In addition to the reductions in PM emissions, air injection improved other operational metrics such as time-to-boil (TTB), firepower (FP), and thermal efficiency. The results in Table 6 are a comparison of 4 air injection tests and 4 baseline tests. Each of these tests uses the same fuel with the same fuel spacer. IWA (International Workshop Agreements) tiers are provided for cold start thermal efficiency and high firepower PM (PM/energy delivered).

Table 6: Cold start test results comparison between baseline and best performing nozzle/flow-rate combination

	5x2mm, 60 SLPM, n=4			Baseline, n=4			
	mean	**Std. Dev.**	**Tier**	**mean**	**Std. Dev.**	**Tier**	**Improvement**
TTB (min)	62.5	1.9		72.8	6.0		14% reduction
Temp. corrected TTB (min)	62.6	1.8		73.1	6.8		14% reduction
Dry Fuel Consumed (g)	3184.4	129.3		3199.8	119.4		0% reduction
FP (kW)	14.2	0.8		12.3	1.4		15% increase
CS Therm. Eff. (%)	45%	2%	4	44%	1%	3	1% increase

PM (mg)	1084.4	223.0		14154.3	2179.9		92% reduction
PM/energy del. (mg/MJd)	45.4	9.4	3.96	601.5	101.1	1	92% reduction

Gravimetric filters from the EC/OC experiments (4.2) were also analyzed. These tests were much shorter than the cold start tests, and are more of a "snap-shot" that captures startup, high firepower, and burn out of roughly 550 grams of fuel in total. The standard deviation of these results are much larger than the cold start tests due to the shorter test length. Even though these tests were much shorter, they still show that air injection is an effective means of reducing particulate matter. All of the nozzles and flow rates tested performed successfully, and significantly reduced the total amount of PM emitted by the stove. Figure 28 shows all of the gravimetric results from EC/OC testing, including baseline and all of the air injection tests.

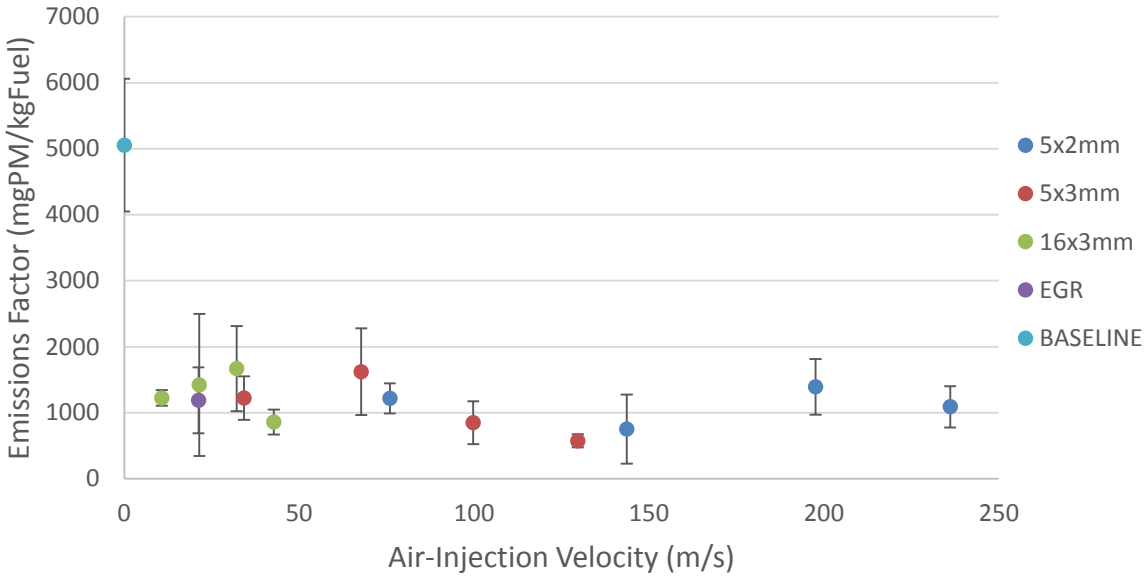

Figure 28: Gravimetric results from EC/OC testing; all nozzles and flow rates significantly reduce total PM when compared to baseline

4.2 EFFECTS OF AIR INJECTION ON ELEMENTAL AND ORGANIC CARBON

Showing statistical difference between EC/OC tests required the use of a two-way analysis of variables (ANOVA) table. A two-way ANOVA table allows one to see if there is a statistical difference in results where there are two variables that can interact with one another. This is appropriate in the case of this work because air injection flow rate and nozzle geometry are both varied. Each two-way ANOVA table created uses a significance level of 20%, which indicates that there is a 20% risk of concluding that an effect exists when there is no actual effect (Minitab Inc., 2016). When reading an ANOVA table, it is important to look at the p-values. If the p-value is less than the significance level it is safe to say that that parameter has a significant effect on the test results. The p-value for both variables and the interaction between the two must be taken into account. If the p-value for the interaction of the two variables is less than the significance level the main effects cannot be interpreted without considering the interaction effect (Minitab Inc., 2016). If the p-value for either of the effects or the interactions thereof are greater than the significance level, then there is no statistical difference in the results between variables. Standard deviations for all of the air injection tests are very large in comparison to the standard deviations seen in cold start test results. This is due to the fact that startup is a much more significant portion of these "snap-shot" tests than it is in a cold start test. For example, startup may take 5 minutes at the beginning of a 65-minute cold start test. The EC/OC tests were much shorter, anywhere from 10-20 minutes. Depending on the air injection flow rate, startup can be faster or slower. At high flow rates starting the stove was difficult because the fire was sometimes blown out, which resulted in more emissions from smoldering fuel. The combination of startup being a more significant portion of total test time, and difficulty starting some of the tests resulted in significant variability in the emissions.

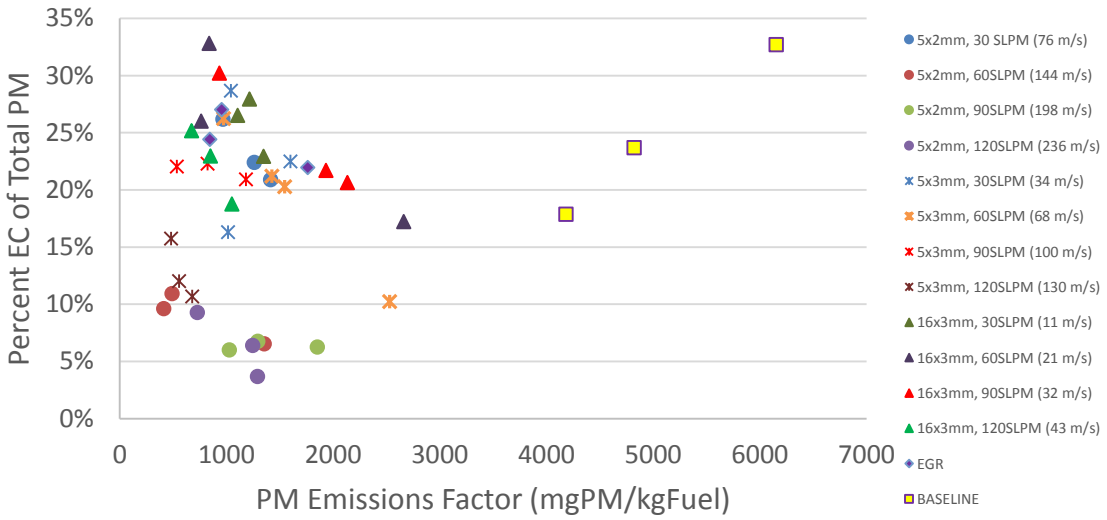

Figure 29: Percent EC of total PM emitted

Figure 29 shows that nozzle geometries that significantly reduce PM do not necessarily significantly reduce EC, and nozzles that significantly reduce EC may not necessarily reduce PM. For example, the 5x2mm nozzle at both 90 and 120 SLPM does not reduce PM or EC as well as the 5x2mm operating at 60 SLPM or the 5x3mm at 120 SLPM. What can be seen is that the velocity of the air being injected has a significant effect on the amount of EC emitted by the stove. Reducing the outlet area of the nozzle increases the velocity of air exiting the nozzle. Nozzle ($p = 8.55 \times 10^{-7}, \alpha = 0.20$), flow rate ($p = 8.9 \times 10^{-4}, \alpha = 0.20$), and the combination thereof ($p = 0.04, \alpha = 0.20$) all have a significant effect on the reduction of EC as a percentage of total PM. Judging from the p-values each parameter has a significant effect. Table 33 in the appendix provides all of the percent EC values for each individual tests. In an effort to calculate the actual nozzle velocity the temperature was assumed to be 600°C at the nozzle exit (see the legend in Figure 29). If graphed against velocity it becomes more apparent that the reduction of EC is driven primarily by velocity.

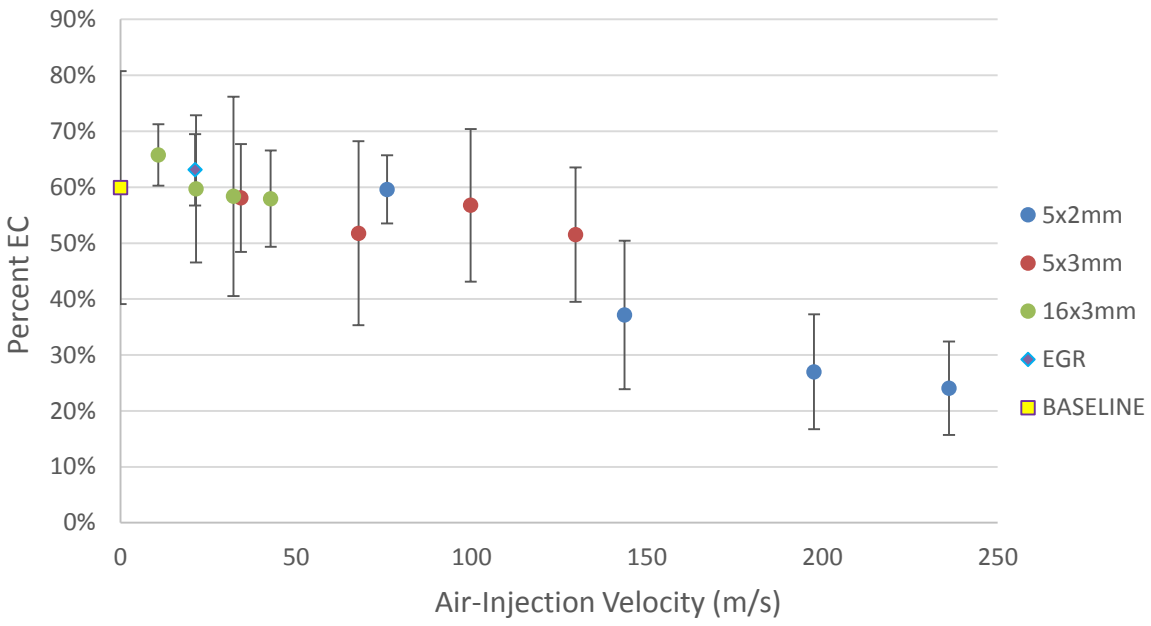

Figure 30: Percent EC of total carbon emitted as a function of air injection velocity

Injection velocity is not the only factor that effects EGR results. EGR recirculates exhaust, which increases the residence time of PM in the combustion chamber. Residence time is not accounted for in Figure 28, Figure 29, Figure 30, Figure 31, or Figure 32. EC/OC decreases in nearly the exact same way as percent EC; the higher velocities resulting from fewer and smaller holes decreases the EC/OC ratio most effectively.

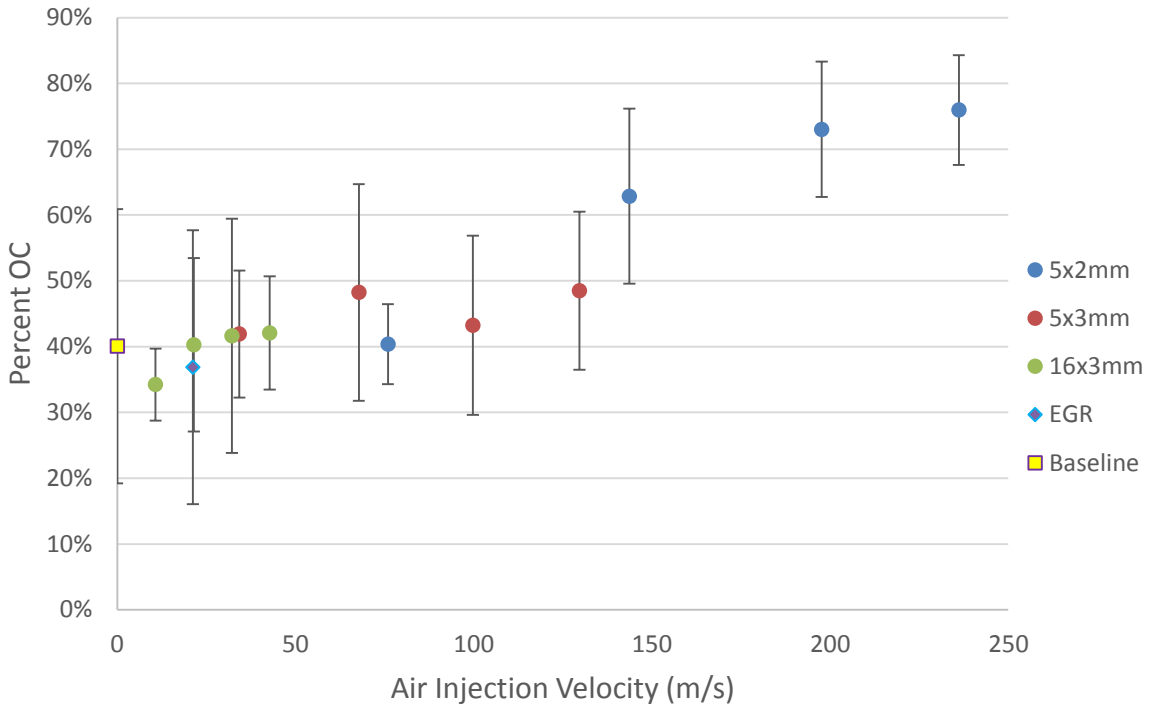

Figure 31: Percent OC of total carbon emitted as a function of air injection velocity

An interesting result from these experiments is that there is no significant difference in the amount of OC produced between flow rates ($p = 0.35$, $\alpha = 0.20$), nozzles ($p = 0.88$, $\alpha = 0.20$), or the interaction between the two ($p = 0.53$, $\alpha = 0.20$). Even though EC shifts dramatically as the injection velocity increases, OC stays relatively constant across flow rates and nozzles. Table 32 provides all of the EC/OC data for individual tests. Table 26, Table 27, Table 28, and Table 29 provide two-way ANOVA tables for EC, OC, EC/OC, and percent EC respectively.

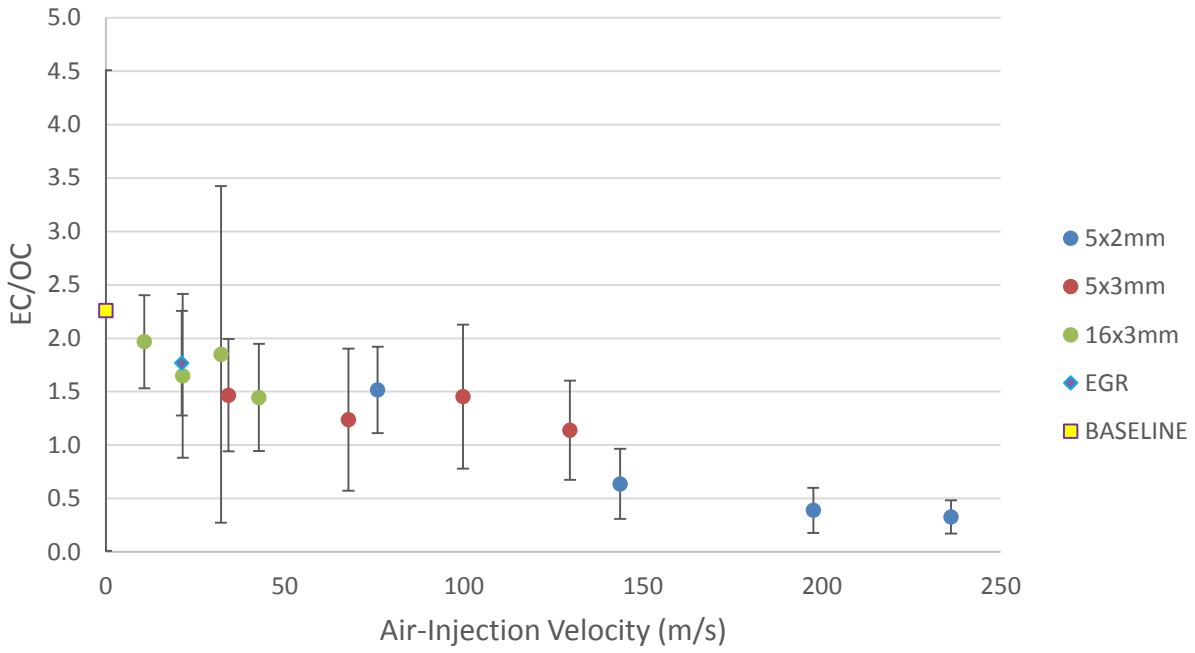

Figure 32: EC/OC ratios from ambient air injection and EGR as a function of velocity

It is clear that the velocity of air leaving the nozzle drives the changes that are causing the decrease in EC. Further, if the velocities and Reynolds (Re) numbers of each test point are compared it can be seen that velocities around 135 m/s and orifice throat Re numbers around 90,000 result in the best EC reduction, and the best overall PM reduction. This can be seen in Figure 29; the 5x2mm operating at 60SLPM and 5x3mm operating at 120SLPM result in similar velocities and Re numbers and produce similar results despite the difference in orifice diameter. Tables 9-21 in the appendix have all of the EC/OC results for each individual test. Additionally, two-way ANOVA tables for total EC, total OC, percent EC, and EC/OC can be found in the appendix. In these ANOVA tables flow rate and nozzle are the two variables. An ANOVA table cannot tell the difference between individual flow rates or nozzles, but it does indicate that either flow rate, nozzle or the interaction thereof has a significant effect on the results. Each ANOVA table uses a significance level of 20% ($\alpha = 0.20$).

Table 7: Variable Effect on EC and OC

α = 0.20	Flow Rate	Nozzle	Interaction
Total EC	$P = 1.8 \times 10^{-5}$	$P = 1.0 \times 10^{-6}$	P = .0056
Total OC	P = 0.35	P = 0.88	P = 0.53
EC/OC	P = 0.21	P = .0046	P = 0.84
Percent EC	P = 0.04	$P = 27 \times 10^{-5}$	P = 0.31

Table 7 shows the p-values that each variable has on EC, OC, EC/OC, and percent EC of total C. As stated previously, the OC emitted by the stove doesn't significantly change between nozzles or flow rates. Since $p < \alpha$, total EC is effected by flow rate, nozzle geometry, and the interaction thereof, so when determining the dominant variable both must be examined to see which is dominant even though both have $p < \alpha$.

4.3 PROTOTYPE AIR-INJECTION SYSTEM

Possibly the most exciting result of this project was the implementation of a functional prototype in Kenya. Designing and building an air injection system for the laboratory resulted in a system that was very easy to operate, and resulted in consistent PM reductions of 92% from baseline testing. The adaptation required to make the leap between the laboratory and field testing was substantial. A prototype could not rely on compressed air and a mass flow controller; it had to operate with little to no user input, rely on an onboard fan, and effectively reduce PM. Using a fan required a nozzle that imposed as little pressure drop as possible, was easily integrated into the existing combustion chamber, and did not severely alter the aesthetics/appearance of the stove.

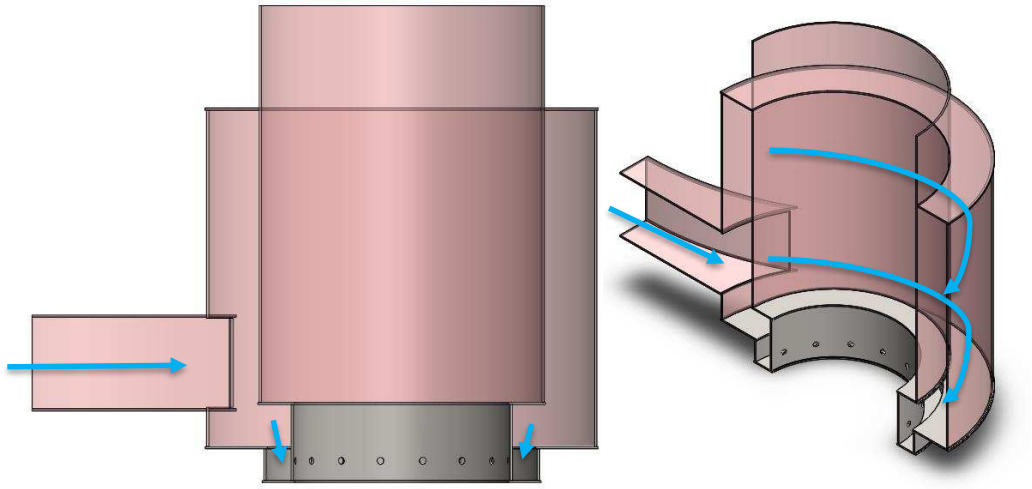

Figure 33: Solidworks rendering of prototype air injection nozzle

Air enters, as indicated by the blue arrows in Figure 33, through the neck and exits through the nozzle into the stove in the same location as the air injection nozzles designed and used in the laboratory. The inner chimney has the same dimensions as the original chimney in the stove (121 mm ID), and fits into the combustion chamber as a "drop-in" replacement for the original chimney. Figure 34 shows a comparison between the original combustion chamber design and the combustion chamber with the prototype air injection nozzle installed.

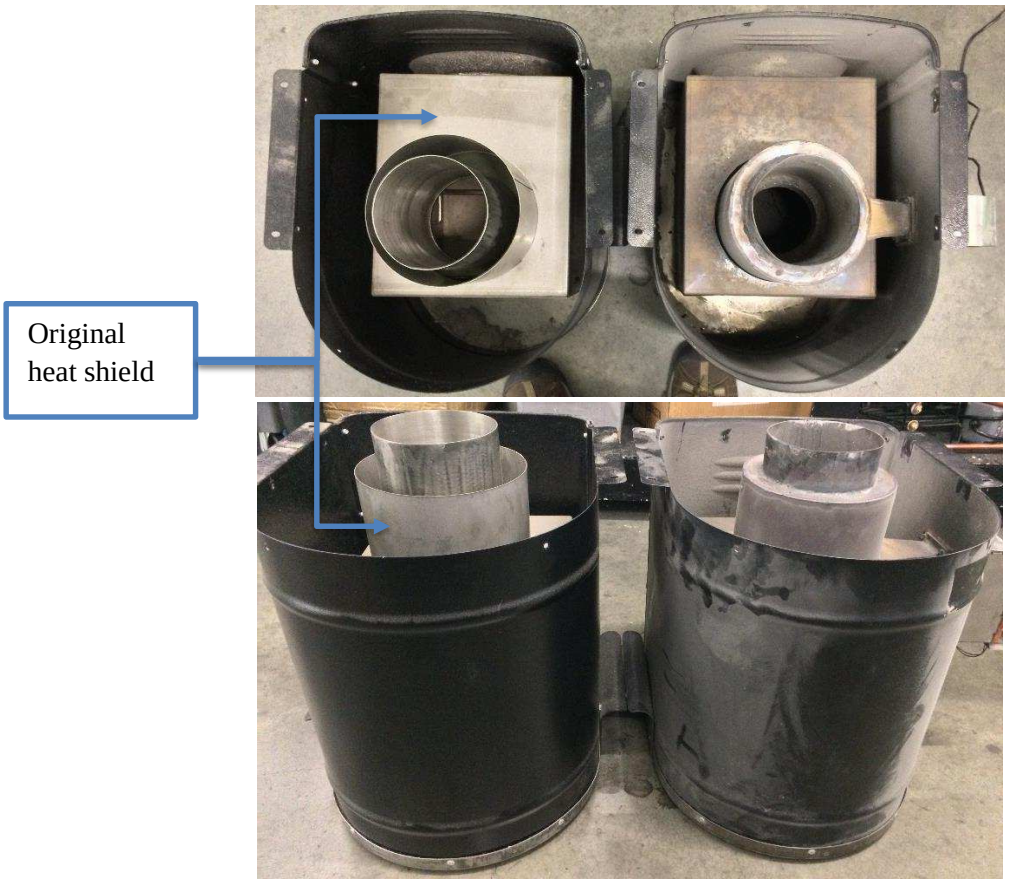

Figure 34: Left - Original combustion chamber, Right - Combustion chamber with prototype nozzle installed

The original stove has a radiation/heat shield that encases the lower chimney and combustion chamber to keep temperatures elevated. The air injection nozzle geometry is meant to be as similar as possible to the original design, so the outside of the ducting is dimensioned such that it is approximately the same size, and sits in the same location as the radiation/heat shield. Making the outside of the nozzle ducting the same dimensions as the radiation/heat shield also increased the volume between the fan and the orifices.

4.3.1 PROTOTYPE NOZZLE SELECTION

As expressed in section 4.2, the prototype nozzle geometry was designed such that it approximates the original geometry of the combustion chamber and adjacent components, while keeping the pressure drop between the fan and nozzle as small as possible. Maintaining a large

volume in the nozzle was an important design consideration. Compared to the nozzle, all other pressure drops through the system are negligible. For example, with the 5x2mm nozzle operating at 60 SLPM the pressure drop through the orifices is approximately 6.5kPa, whereas the pressure drop leading up to the nozzle is 0.001kPa. This is assuming the dimensions of the tube leading to the nozzle are 0.3m long and 0.0381m in diameter. From this point on, designing the prototype consisted of matching fan performance curves to the pressure required for different nozzles.

After evaluating all of the nozzles in a laboratory test setup it was clear that the 5x2mm nozzle operating at 60 SLPM offered the best PM reduction. However, the pressure drop imposed by this nozzle was too great for a low cost fan to overcome. Keeping cost in mind, it was not practical to use this nozzle with a DC fan. A trade study was conducted to match one of the nozzles tested with a cheap, low power DC fan that could provide adequate flow. Several fans were selected, and their pressure curves were digitized. These digitized pressure curves were superimposed onto a system pressure curve developed for each individual nozzle. With the superimposed pressure curves, it was then possible to choose a fan and nozzle combination such that the fan was capable of providing the flow required for that nozzle's best PM reduction operating point. The nozzle chosen for the prototype was the 16x3mm nozzle. The 16x3mm nozzle showed similar PM reductions compared to the 5x2mm nozzle, and has a much lower pressure drop. The 16x3mm nozzle shows significant PM reductions at and above 100 SLPM with the most significant reduction at 120 SLPM. Figure 35 shows the final fan performance curve with the system curve superimposed; the operating point shown is where the blue line intersects with the 12V performance curve.

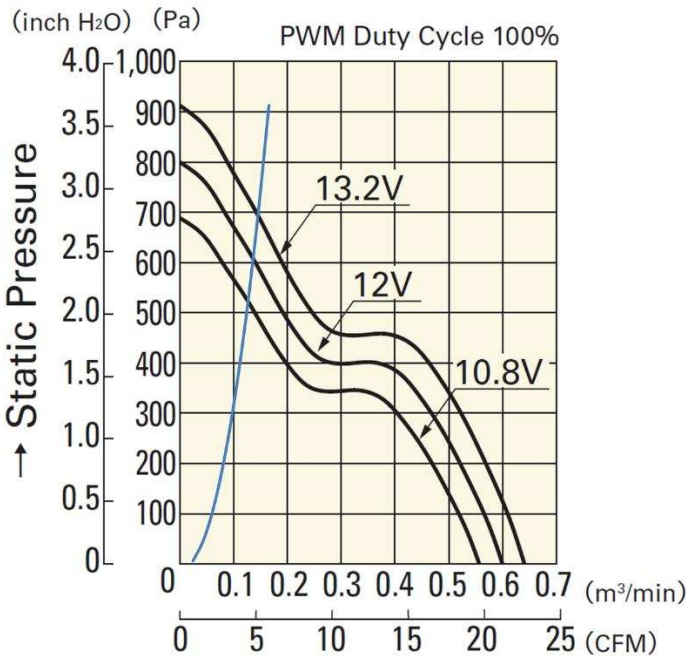

Figure 35: Performance curve for prototype air injection fan (Mouser Electronics, 2016) with system pressure curve in blue.

The desired flow rate for the 16x3mm nozzle is 120 SLPM. Referring to Figure 21 in section 3.6, 120 SLPM at local temperature and pressure is approximately 140 LPM. The operating point shown in Figure 35 indicates that the chosen fan can provide approximately 130 LPM, which satisfies the flow requirement for significant PM reductions. Calculations for the pressure drop across the nozzle orifices can be found in the appendix. As stated previously, the orifices dominate the pressure drop through the system. All other major/minor losses are negligible in comparison. Calculations for this pressure drop can be found in the appendix, Figure 41.

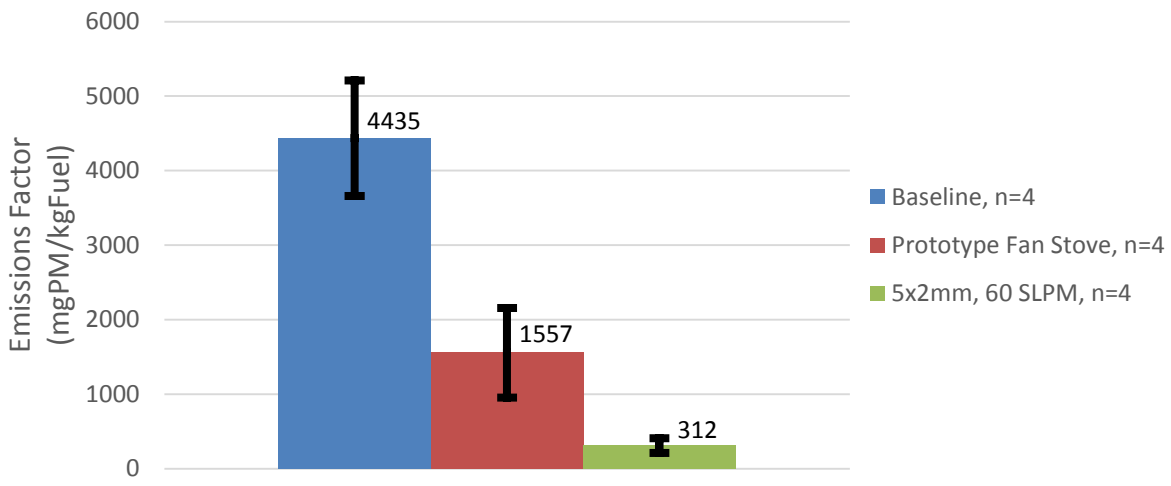

Figure 36: Emissions Factors for Baseline, Prototype Fan Stove, & 5x2mm Air-Injection Nozzle

Figure 36 compares the PM emission factors for the prototype fan stove to both baseline and the 5x2mm nozzle operating at 60 SLPM. Although the prototype did not perform as well as the 5x2mm nozzle operating at 60 SLPM, it still significantly reduced PM emissions compared to baseline.

4.4 PROTOTYPE THERMOELECTRIC GENERATOR MODULE

Steady, reliable electricity is a scarce commodity in the developing world; the development of a low cost, chimney mounted thermoelectric power generator (TEG) was proposed as an innovative system component that could power the air injection system. The concept is to use TEG modules coupled with heat capture and heat rejection devices to harvest waste energy from the stove's exhaust. The goal was to develop a power module that was capable of providing enough power for the forced air injection system (section 4.3), and enough additional power for a 5 volt USB port that stove users could use for charging, lighting, a radio, or other simple electronic devices that a 5 volt USB port could successfully support. The addition of the USB port is meant to serve as an incentive to consumers to adopt emissions reduction technology.

Rather than walking to a charging station and paying to charging their device, stove users could simply plug their device into the power module while cooking.

This idea was carried from a concept to a prototype, which was deployed in Kenya (with the prototype air-injection system discussed in 4.3) to received user feedback on the design. The idea/product was also pitched at the MIT Clean Energy Prize and received the $15,000 Energy For Development prize, which spawned the creation of a start-up company, $\dot{Q}apture$. Currently, $\dot{Q}apture$ is in search of further funding to explore the technological feasibility of what the pilot innovation fund has provided as a proof of concept.

4.4.1 DESIGN, FABRICATION, AND TESTING

The chimney is an attractive location for a power module; rather than designing stove specific power modules, one module was developed as a universal drop-in addition that could be easily adapted to any chimney stove. The Envirofit EFI – 100L Institutional was again used a development platform. Using the flow measurements discussed in 3.3, it was estimated that approximately 1.7 kW of energy is rejected to the ambient environment through the chimney when the temperature difference (dT) is approximately 200K ($T_{fluegas} = 500K \; and \; T_{ambient} = 300K$). TEG's are notoriously inefficient; 2-3% efficiency is considered successful (Tellurex, 2010). Optimistically assuming 4.5% efficiency, it is possible to extract approximately 75 watts of energy from the chimney by using TEG's.

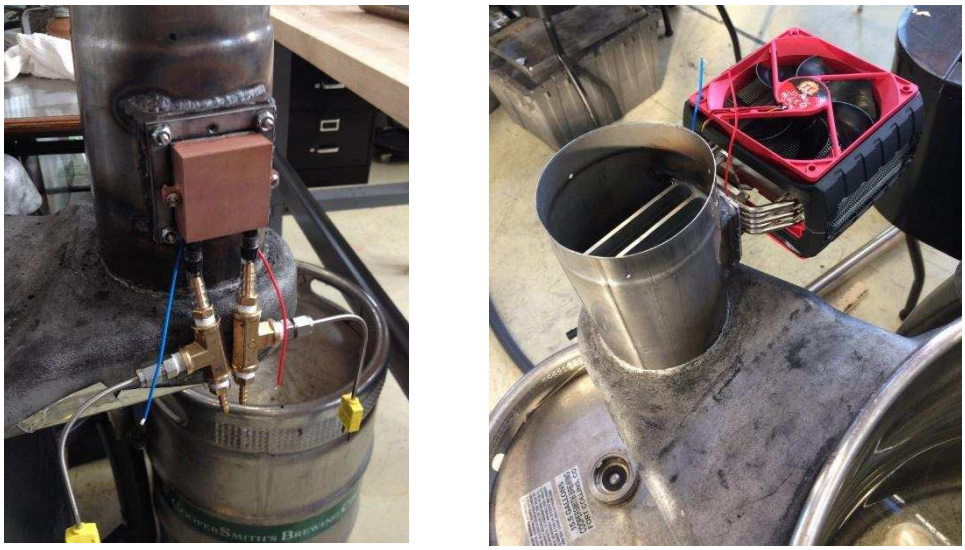

Figure 37: Left - Laboratory prototype with water cooler, Right - Laboratory prototype with CPU cooler

The laboratory prototype seen in Figure 37 used both liquid cooling and a heat-pipe heat sink that is meant for cooling computer CPU's. The water cooler is designed specifically for TEG modules. A small pump was used to circulate ice water through the copper water block, which resulted in a TEG cold side temperature between 1-6°C. Using a Marlow Industries TG12-8-01LS (7.95W) module and a constant resistance (2.9Ω) load, power output was consistent at roughly 4W and peaked at just over 5W. The CPU cooler (right side, Figure 37) did not perform as well as the water block. With the same heat sink used for heat capture, and the same constant resistance (2.9Ω) load it was able to maintain a power output between 1.5-1.8W. Graphs of both power and flue gas temperature for both of the laboratory prototype set ups can be found in the appendix, Figure 42 and Figure 43. Although the water block performed the best, it requires a reservoir for water circulation, which is not feasible from an end user standpoint. Using the water block did help narrow in on the fact that heat capture in the chimney is more difficult than heat rejection. Table 8 provides test results for the laboratory prototype.

Table 8: Performance results for laboratory prototype chimney mounted TEG module

	Average Module dT	Average Hot Side Temperature (°C)	Average Module Power (W)
Laboratory prototype: single elliptical fin, Marlow TG12-8-01LS, water block	103.9	111.9	3.0
Laboratory prototype: single elliptical fin heat capture, Marlow TG12-8-01LS, water block heat rejection, 60 SLPM forced air-inj.	84.7	90.5	2.1
Laboratory prototype: 3-fin heat capture, Marlow TG12-8-01LS, water block heat rejection	134.5	142.3	4.6
Laboratory prototype: 3-fin heat capture, Marlow TG12-8-01LS, water block heat rejection, 60 SLPM forced air-inj.	124.5	131.6	4.0

The field prototype utilized a more effective heat capture heat sink, and an air cooled heat rejection system. The air cooled heat rejection system uses a 0.5W fan to force air over a bonded-fin heat sink. This alternative was chosen over the water cooled system because of its simplicity and low power requirement. It proved effective, maintaining the cold side of the module at roughly 70°C. This is better than some of the existing cookstove TEG power modules currently on the market, which use boiling water as a heat rejection method.

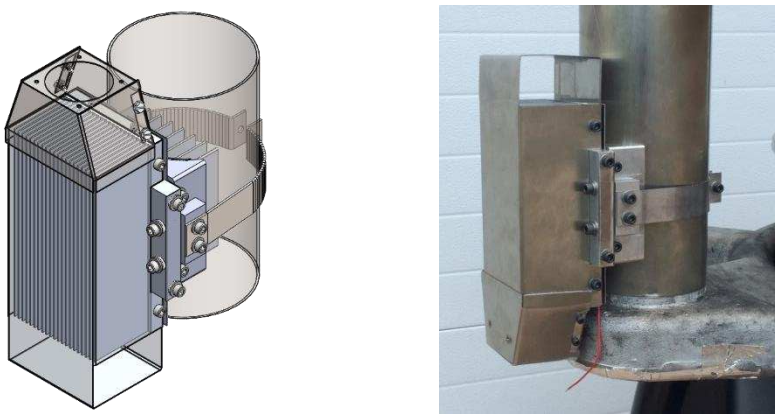

Figure 38: Left - CAD rendering of field prototype, Right - Functional field prototype

Figure 38 shows the field prototype. In an effort to increase power output, a larger TEG module (Custom Thermoelectric 2411G-7L31-15CX1) with a maximum power output rated at 22 watts was chosen for use in this prototype. This module performed at approximately half of its rated output for the measured temperature difference across the module; it produced approximately 1 watt with a module dT of 90°C. Figure 44 in the appendix shows a graph of the TEG power module output with a graph of the manufacturer power output specifications. At the dT which the module is operating during the test it should be producing approximately 2 watts. Although the field prototype did not perform well, it was sent to Kenya to accommodate the prototype emissions reduction system and gain user feedback on the concept of a chimney mounted TEG power module. The concept was well received; stove users liked the idea of have a small power supply in the kitchen. However, many users raised the point of charging a phone/device in the vicinity of a stove. Charging a device near an institutional cookstove means charging a device near a very hot stove with a boiling pot of water, neither of which complement the lifecycle of electrical devices. Table 9 provides the performance results from testing the field prototype. Limited data was obtained for the field prototype; it was only tested once with the prototype forced air injection system before being shipped to Kenya for field testing.

Table 9: Performance results for field prototype chimney mounted TEG module

Average HS Temperature (°C)	Average CS Temperature (°C)	Average Module dT
134.3	69.3	65.0
Maximum HS Temperature (°C)	**Maximum CS Temperature (°C)**	**Maximum dT**
169.3	84.4	88.2
Minimum HS Temperature (°C)	**Minimum CS Temperature (°C)**	**Minimum dT**
54.3	38.8	15.5
Average Power (W)	**Maximum Power (W)**	
0.59	1.05	

4.4.2 TEG POWER MODULE CONCLUSION AND FUTURE WORK

Both of the prototype power modules developed for this project prove that it is certainly possible to recover waste energy from chimney stove exhaust. The limiting factor, at least for the Envirofit EFI – 100L Institutional, is the chimney location with respect to the combustion chamber. At the base of the chimney flue gas temperatures range from 230-250°C, which simply is not hot enough for TEG modules to be effective. Hot side temperatures for the laboratory and field prototypes were approximately 140°C and 134°C on average, respectively. Using the water block with ice-water for heat rejection resulted in an average TEG module temperature difference of 137°C, whereas the air cooled TEG module dT was 65°C on average. It is important to note here that the field prototype was only tested once with the prototype air injection system running, and immediately shipped to Kenya. These two prototypes were tested together due to time constraints. Testing with the air injection system running produces very different results compared to testing without air injection; air injection drastically cools the exhaust stream, resulting in lower hot side TEG temperatures. The difference between tests with and without forced air injection can be seen in Figure 45, Figure 46, Figure 47, and Figure 48 in

the appendix. These tests compared two heat capture heat sinks both with and without forced air injection. The water block was used for heat rejection in all of these tests.

Future work on a chimney mounted TEG power module should include more than one module. The two prototypes were produced with the minimum possible TEG modules in an effort to keep costs down. The flue gas temperatures are not high enough for a single TEG module to power the air injection system and a USB port. To successfully extract enough power from the flue gas to supply both the air injection system and a USB port multiple TEG modules will be required. Another issue that will require future work is fin fouling. The amount of soot that accumulates on the heat capture heat sink is significant, and effectively acts as insulation that impedes heat transfer to the TEG module. This was tested by using a propane burner to keep exhaust gas temperatures at approximately 230°C with the TEG power module in place after it had significant fouling. After testing the TEG power module with the fouled fins, it was removed and cleaned for another test with the propane burner. The fouling resulted in a 24% decrease in average power output from the TEG power module. This is a significant difference considering that the fouled heat sink had only 7 hours of high firepower exposure. Results from this test, and a picture of the test set up can be seen in Figure 49 and Figure 50 in the appendix.

4.5 CONCLUSIONS

This investigation measured the effects of forced air injection on PM emissions and EC/OC from an institutional chimney stove. The use of forced air injection on institutional chimney stoves results in reductions up to 92% in overall PM emissions. As shown in Figure 28, all of the air injection tests showed significant reductions in PM. The emissions factors resulting from the use of forced air injection depend on both nozzle geometry and the air injection flow rate. Nozzles with fewer and smaller holes show significant reductions in PM at lower air injection

mass flow rates but may be limited in applicability due to fan curves. The lower total area of the orifices on nozzles such as the 5x2mm result in exit velocities much higher than nozzles such as the 16x3mm. Air injection velocities and Re numbers (measured in the throat of the orifice) were approximately 144 m/s and 95,000 for the 5x2mm at 60 SLPM and approximately 130 m/s and 84,000 for the 5x3mm at 120 SLPM. These two nozzles produced similar results in terms of overall PM and EC reduction. These reductions could be the result of jet in cross flow (JICF) mixing, where horseshoe vortices and counter-rotating vortex pairs are created. Enhanced mixing of fuel and oxidizer is believed to be the primary mechanism by which overall PM and EC are reduced. Each nozzle has a certain flow rate at which it reduces PM most significantly, but air injection has an entirely different relationship with EC and OC.

The most significant reductions in EC are seen at the highest injection velocities tested, the 5x2mm nozzle operating at 120 SLPM. At this operating point the injection velocity is approximately 240 m/s, which resulted in 24% EC. Compared to baseline tests, which produced 60% EC, this is a significant reduction. Figure 30 shows the trend between injection velocity and percent EC. Significant reductions in EC are not clear until the air injection velocity reaches approximately 140 m/s. It is clear from this graph that a more turbulent combustion chamber results in better EC reductions. This is an interesting point that warrants further investigation: even though some nozzle configurations result in significant PM reduction, such as the 16x3mm operating at 120 SLPM, they may not shift the EC/OC ratio towards a higher OC content, which would give the emissions a net cooling effect rather than a net warming effect on the climate. Another interesting point is that OC is not significantly changed by air injection. EC/OC decreases as injection velocity goes up because of the decrease in EC rather than any significant increase in OC. EC and OC reduction mechanisms clearly are not the same.

Implementing forced air injection systems on institutional chimney stoves could significantly reduce PM, EC, and SLCF emissions. Implementation could come in the form of a built in system, such as the prototype developed in this project, or a kit that can be adapted to multiple stoves. An important consideration when implementing this technology is the effect of air injection on particle size distribution. Shifting the particle size distribution to ultrafine particles ($PM_{0.1}$) could have detrimental effects on both human health and the environment. However, particle size distribution was not part of this investigation, and it cannot be concluded from these results whether or not this air injection method affects particle size. Laboratory results were possible with the use of compressed air, normalized fuel, and otherwise essentially perfect operating conditions. This investigation established a relationship between forced air injection and PM reduction, as well EC/OC. The results of this investigation are conclusive in that forced air injection successfully reduces both PM and EC, but also raise further questions about resulting chemical kinetics, PM and EC reduction mechanisms, and the fluid dynamics that encompass this particular set of JICF scenarios.

4.6 FUTURE WORK

Future work could start with the completion of the same EC/OC test matrix, but with cold start tests rather than the "snap-shot" tests performed for this investigation. The short tests were sufficient for establishing a relationship between forced air injection and the EC/OC ratio, but don't truly reflect the operation of institutional stoves the way cold start tests do. Completing the test matrix this way would have been ideal, but not feasible due to time constraints. A test matrix this extensive would also provide better resolution on overall PM emissions. In addition to the longer tests, it would be beneficial to measure and record temperatures in and around the air injection nozzle, and the combustion chamber. Knowing the temperature of air just as it exits

the nozzle would allow for a better understanding of the thermodynamics that could be affecting PM or EC reductions. For example, the temperature of air exiting the nozzle was estimated for this project to be 600°C. This is believed to be a reasonable estimate; if the air exiting the nozzle were the same as known combustion chamber temperatures (approximately 850°C) it would result in a choked flow condition because of the rapid change in density. Knowing the temperature of air in the nozzle and just as it exits would provide insight into the fluid dynamics occurring, and thus the combustion/chemical kinetics at play.

Future work should also include significant effort into simulating chemical kinetics which result from using air injection. Although air injection has been proven successful, the fundamental combustion mechanisms have not been thoroughly investigated. Understanding the chemical kinetics will lead to a better understanding of why air injection is reducing EC more significantly than OC, and why overall PM is reduced. Combustion models should include JICF scenarios that adequately describe the air injection nozzles in this investigation, particularly the nozzles that resulted in high air injection velocities. Modified combustion efficiency (MCE) should also be measured in future testing, and compared to MCE estimated by modeling chemical kinetics. A better understanding of how air injection affects MCE could provide insight into the production/reduction of both EC and OC. The results of these experiments show that EC is reduced as air injection velocity increase. However, they do not show whether or not the production of EC is being limited, or EC is being reduced after it is produced. Once these mechanisms are better understood, this technology can be better adapted to other types of stoves.

This investigation tested the effects of forced air injection on a single stove. To gain a better understanding of the implications of air injection on a global scale it needs to be adapted to and tested on multiple chimney stoves. For example, there are far more plancha style chimney stoves

in the world than there are institutional chimney stoves. These stoves have a much different style of combustion chamber, which will require a redesign of the nozzle for proper placement in the stove. The Advanced Biomass Combustion Laboratory has the knowledge and capability to examine this technology as it applies to multiple cook stoves, gasifiers, pellet stoves, and solid fuel stoves used primarily for heating. If this technology is not reliant on stove type it would open up the possibility for implementation on many different kinds of solid fuel combustion devices. Developing this technology for different stove types may require significant adaptation of the nozzle geometry.

As a result of the EC/OC testing, a certain range of nozzle outlet velocities and Re numbers were identified to significantly reduce both EC emissions and overall PM emissions. If better understanding of the temperatures and pressures in and around the injection nozzle are secured, it will be possible to develop a test matrix based not on nozzle geometry or flow rate, but instead on air injection velocity and/or Re number. If it is indeed the case that the reduction of overall PM and EC is dependent on injection velocity, then it could be possible to develop much simpler nozzles that are just as effective at reducing harmful emissions.

Particle sizing is another issue that needs to be addressed. Recent work (Rapp, Caubel, Wilson, & Gadgil, 2016) suggests that forced air injection shifts particle size distribution to ultrafine particles, which could have detrimental effects on human health and the environment. The tests conducted by Rapp et al. were on residential cookstoves, and found reductions in PM up to 66%. Testing forced air injection on an institutional cookstove at CSU's Advanced Biomass Combustion Laboratory resulted in up to 92% reductions in overall PM from baseline tests. These tests did not include any investigation into particle size distribution. Although

overall PM mass is significantly decreased, it is possible that there could be a high quantity of low mass particles emitted.

BIBLIOGRAPHY

Advanced Biomass Combustion Laboratory, Colorado State University. (2015). Executive Summary: Pilot Innovation Fund III. Fort Collins, CO, USA.

Alicat Scientific. (2016). *Alicat Scientific*. Retrieved from Alicat Scientific: https://www.alicat.com/

Bailis, R., Drigo, R., Ghilardi, A., & Masera, O. (2015, January 19). The carbon footprint of traditional woodfuels. *Nature Climate Change, 5*, 266-272. doi:10.1038/NCLIMATE2491

Bond, T. C., Bhardwaj, E., Dong, R., Jogani, R., Jung, S., Roden, C., . . . Trautmann, N. M. (2007, 05 30). Historical emissions of black and organic carbon aerosol from energy-related combustion, 1850-2000. *Global Biogeochemical Cycles, 21*, 1-16. doi:10.1029/2006GB002840

Bond, T. C., Doherty, S. J., Fahey, D. W., Forster, P. M., Berntsen, T., DeAngelo, B. J., . . . Zender, C. S. (2013, June 6). Bounding the role of black carbon in the climate system: A scientific assessment. *JOURNAL OF GEOPHYSICAL RESEARCH: ATMOSPHERES, 118*, 5380-5552. doi:10.1002/jgrd.50171

Bonjour, S., Adair-Rohani, H., Wolf, J., Bruce, N. G., Mehta, S., Pruss-Ustun, A., . . . Smith, K. R. (2013). Solid Fuel Use for Household Cooking: Country and Regional Estimates for 1980-2010. *Environmental Health Perspectives, 121*(7), 784-790. Retrieved 08 23, 2016, from https://www.ncbi.nlm.nih.gov/pmc/articles/PMC3701999/pdf/ehp.1205987.pdf

Butler, O. R. (n.d.). *SMOKE GETS IN YOUR EYE: THE DEVELOPMENT OF THE HOUSE CHIMNEY*. Retrieved from Ultimate History Project: http://www.ultimatehistoryproject.com/chimneys.html

Custom Thermoelectric. (2014). TEG Specification Sheet Part #: 2411G-7L31-15CX1. Maryland, USA.

Dischino, K. (2015). *METHODS FOR PARTICULATE MATTER EMISSIONS REDUCTION IN WOOD BURNING COOKSTOVES.* Colorado State University, Mechanical Engineering. Fort Collins, CO: Colorado State University.

EPA. (2016, September 12). *Particulate Matter (PM) Basics*. Retrieved from Environmental Protection Agency: https://www.epa.gov/pm-pollution/particulate-matter-pm-basics

Fitz, D. R. (2007, 10 31). *Final Report: Evaluation and Minimization of Organic Aerosol Sampling Artifacts Using Impactors and Quartz Fiber Filter Denuders.* University of California - Riverside. EPA. Retrieved 1 6, 2017, from environmental Protection Agency: https://cfpub.epa.gov/ncer_abstracts/index.cfm/fuseaction/display.highlight/abstract/6242/report/F

Global Alliance for Clean Cookstoves. (2014, 03 19). *technology-and-fuels/testing/protocols.* Retrieved from www.cleancookstoves.org: http://cleancookstoves.org/technology-and-fuels/testing/protocols.html

Global Alliance for Clean Cookstoves. (2016, 08 27). *Impact areas - Women.* Retrieved from www.cleancookstoves.org: http://cleancookstoves.org/impact-areas/women/

Hinds, W. C. (1999). *Aerosol Technology* (2 ed.). Hoboken, New Jersey, USA: John Wiley & Sons, Inc. Retrieved 11 10, 2016

Hussain, J., Palaniradja, K., alagumurthi, N., & Maninaran, R. (2012). Effect of Exhaust Gas Recirculation (EGR) on Performance and Emission characteristics ofa Three Cylinder Direct Injection Compression Ignition Engine. *Alexandria Engineering Journal, 51*(4), 241-247.

IPCC. (2013). *Anthropogenic and Natural Radiative Focing. In: Climate Change 2013: The Physical Science Basis. Contribution of Working Group 1 to the Fifth Assessment Report of the Intergovernmental Panel on Climate Change.* Cambridge, United Kingdom and New York, NY, USA: Cambridge University Press.

Junker, C., & Liousse, C. (2008, 03 03). A global emission inventory of carbonaceous aerosol from historic records of fossil fuel and biofuel consuption for the period 1860-1997. *Atmospheric Chemistry and Physics, 8*, 1195-1207. Retrieved 08 01, 2016, from www.atmos-chem-phys.net/8/1195/2008/

Kodros, J. K., Scott, C. E., Farina, S. C., Lee, Y. H., L'Orange, C., Volckens, J., & Pierce, J. R. (2015). Uncertainties in global aerosols and climate effects due to biofuel emissions. *Atmospheric Chemistry and Physics*, 8577-8596.

Kopp, R. E., & Mauzerall, D. L. (2010, 06 29). Assessing the climatic benefits of black carbon mitigation. (W. L. Chameides, Ed.) *PNAS, 107*(26), 11703-11708. Retrieved 08 01, 2016, from www.pnas.org/cgi/doi/10.1073/pnas.0909605107

Lamarque, J. F., Bond, T. C., Eyring, V., Granier, C., Heil, A., Klimont, Z., . . . van Vuuren, D. P. (2010, 08 03). Historical (1850-2000) gridded anthropogenic and biomass burning emissions of reactive gases and aerosols: methodology and application. *Atmospheric Chemistry and Physics, 10*, 7017-7039. doi:10.5194/acp-10-7017-2010

Lee, C. M., Chandler, C., Lazarus, M., & Johnson, F. X. (2013). *Assessing the Climate Impacts of Cookstove Projects: Issues in Emissions Accounting.* Stockholm Environmental Institute. Stockholm: Stockholm Environmental Institute. Retrieved 08 01, 2016, from www.sei-international.org

Lighty, J. S., Veranth, J. M., & Sarofim, A. F. (2011, Dec 27). Combustion Aerosols: Factors Governing Their Size and Composition and Implications to Human Health. *Journal of the Air & Waste Management Association*, 1565-1618. doi:10.1080/10473289.2000.10464197

L'Orange, C. (2015, 06 11). Standard Operating Procedure - Gravimetric Filter Handling. Fort Collins, Colorado, USA.

L'Orange, C., Volckens, J., & DeFoort, M. (2012, september 18). Influence of stove type and cooking pot temperature on particulate matter emissions from biomass cook stoves. *Energy for Sustainable Development*, 448-455.

Marlow Industries. (2016, 11 17). Retrieved from www.marlow.com: http://www.marlow.com/

Minitab Inc. (2016, 11 22). *Minitab Express Support*. Retrieved from Minitab Support: http://support.minitab.com/en-us/minitab-express/1/help-and-how-to/modeling-statistics/anova/how-to/two-way-anova/interpret-the-results/key-results/

Morgan, L. (n.d.). *Historic Kitchens*. Retrieved 12 07, 2016, from Home Things Past: http://www.homethingspast.com/historic-kitchen-visit/

Mouser Electronics. (2016). San Ace 38. Mansfield, Texas, USA.

NASA. (2016, 11 28). *Global Climate Change*. Retrieved from NASA: http://climate.nasa.gov/evidence/

Navidi, W. (2011). *Statistics for Engineers and Scientists* (3rd ed.). New York, New York, USA: McGraw-Hill.

Pheng, L. S. (2004). Techniques for environmental control and structural integrity of buildings in ancient China. *Structural Survey, 22*(5), 271-281.

Ramanathan, V., & Carmichael, G. (2008, 04). Global and regional climate changes due to black carbon. *Nature Geoscience, 1*, 221-227. Retrieved 07 29, 2016, from www.nature.com/naturegeoscience

Rapp, V. H., Caubel, J. J., Wilson, D. L., & Gadgil, A. J. (2016, 06 27). Reducing ultrafine particle emissions using air injection in wood-burning cookstoves. *Environmental Science & Technology*, 1-29. Retrieved 07 05, 2016, from http://pubs.acs.org

Rehman, I. H., Ahmed, T., Praveen, P. S., Kar, A., & Ramanathan, V. (2011, 07 25). Black Carbon emissions from biomass and fossil fuels in rural India. *Atmospheric Chemistry and Physics, 11*, 7289-7299. Retrieved 08 01, 2016, from www.atmos-chem-phys.net/11/7289/2011/

Russell, L. M. (2003). Aerosol Organic-Mass-toOrganic-Carbon Ratio Measurements. *Environmental Science & Technology, 37*, 2982-2987. doi:10.1021/es026123w

Schnieder, J., Weimer, S., Drewnick, F., Borrmann, S., Helas, G., Gwaze, P., . . . Kirchner, U. (2006). Mass spectrometric analysis and aerodynamic properties of various types of combustin-related aerosol particles. *International Journal of Mass Spectrometry*, 37-49.

Tellurex. (2010). *Thermoelectric Power Generators.* Retrieved from Tellurex: http://tellurex.com/wp-content/uploads/2014/03/seebeck-faq.pdf

United Nations. (2014). *Kyoto Protocol*. Retrieved from United Nations Framework Convention on Climate Change: http://unfccc.int/kyoto_protocol/items/2830.php

United States Environmental Protection Agency. (2012). *Report to Congress on Black Carbon.* Retrieved June 10, 2016

Watson, J. G., Chow, J. C., & Antony Chen, L.-W. (2005). Summary of Organic and Elemental Carbon/Black Carbon Analysis Methods and Intercomparisons. *Aerosol and Air Quality Research, 5*, 65-102.

White, F. M. (1999). *Fluid Mechanics* (4 ed.). New York City, New York, USA: The McGraw-Hill Companies, Inc. Retrieved 2016

WHO. (2006). *Fuel for Life: Household Energy and Health.* Geneva, Switzerland: World Health Organization. Retrieved 08 27, 2016

WHO. (2014, 01 01). *Burden of disease from the joint effects of Household and Ambient Air Pollution for 2012.* Retrieved from www.who.int/phe: http://www.who.int/phe/health_topics/outdoorair/databases/AP_jointeffect_BoD_results_March2014.pdf

World Health Organization. (2015). *Reducing Global Health Risks Thruogh Mitigation of Short-Lived Climate Pollutants.* Geneva, Switzerland: World Health Organization.

APPENDIX

Stoichiometric Combustion of Wood:

Chemical composition of wood by weight (%)	
Carbon	50
Hydrogen	7
Oxygen	43

$$X = \frac{50}{MW_C} = 4.167$$

$$Y = \frac{7}{MW_H} = 7$$

$$Z = \frac{43}{MW_O} = 2.6875$$

$$aC_xH_yO_z + b(O_2 + 3.76N_2) \rightarrow dCO_2 + eH_2O + gCO + b(3.76N_2)$$

$$4.167a = d + g$$

$$7a = 2e$$

$$2.6875a + 2b = 2d + e + g$$

$$\dot{m}_{stoichiometric\ air} = b\left[\frac{kmol}{s}\right](2 * MW_O + 3.76 * 2 * MW_N)$$

Where:

$$MW_O = 16\ \frac{kg}{kmol}$$

$$MW_N = 14\ \frac{kg}{kmol}$$

$$MW_H = 1\ \frac{kg}{kmol}$$

$$MW_C = 12\ \frac{kg}{kmol}$$

Excess Air:

Stoichiometric Oxygen (%) = Ambient Oxygen (%) – Measured Oxygen (%)

$$Excess\ Air\ Ratio\ (EAR) = \frac{Measured\ Oxygen}{Stoichiometric\ Oxygen}$$

$$\dot{m}_{excess\ air} = EAR * \dot{m}_{stoichiometric\ air}$$

$$\dot{m}_{total\ air} = \dot{m}_{stoichiometric\ air} + \dot{m}_{excess\ air}$$

Figure 39: Process for calculating the flow through the stove

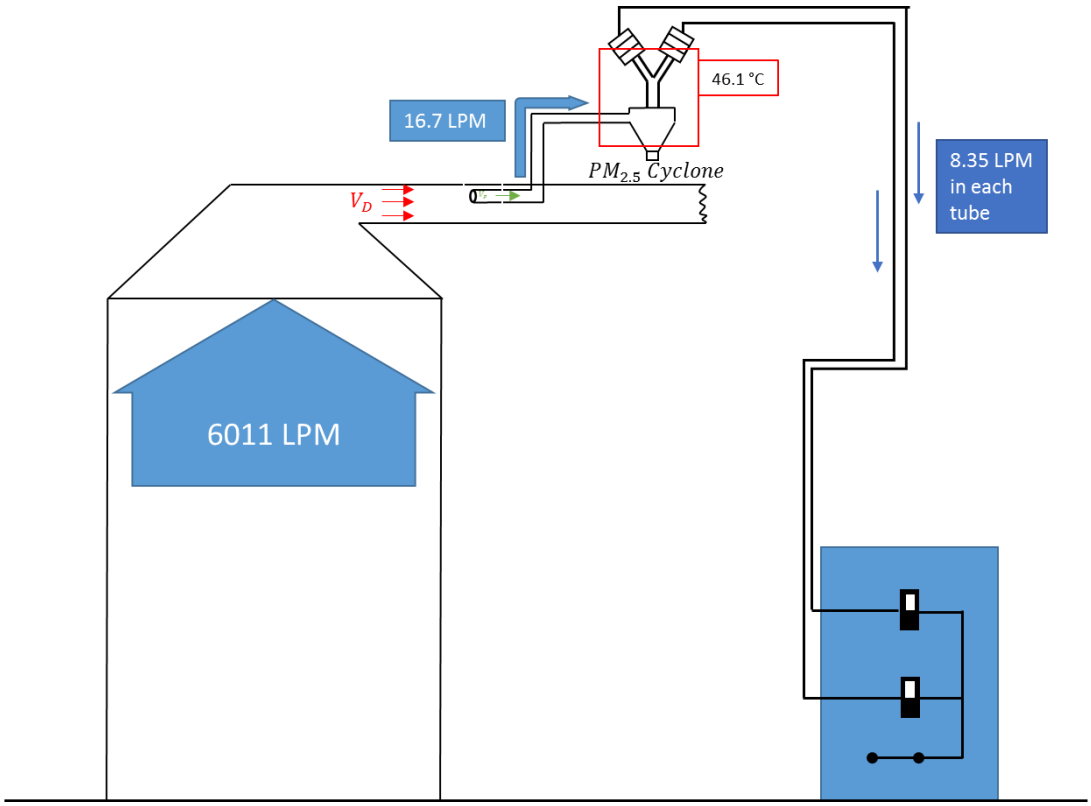

- Hood Duct
  - 0.12344 m ID
  - $A_D = 11.97 \times 10^{-3} m^2$
- Isokinetic Probe
  - 0.0065278 m ID
  - $A_P = 33.47 \times 10^{-6}\ m^2$
  - $Q_P = 16.7\ \frac{L}{60s}\ \times\ \frac{m^3}{1000L} = 27.83\ \times 10^{-5}\ \frac{m^3}{s}$
- Duct Flow Rate
  - Blower Speed = 1340 RPM
  - $4485.49 \times 10^{-6}\ \frac{m^3}{rev}$
  - $1340\ \frac{rev}{60s}\ \times 4485.49 \times 10^{-6}\ \frac{m^3}{rev} = Q_D = 6011\ LPM =\ 0.1002\ \frac{m^3}{s}$
- Velocity in Duct
  - $Q_D = V_D A_D$
  - $V_D = 8.37\ \frac{m}{s}$
- Velocity in Probe
  - $Q_P = V_P A_P$
  - $V_P = 8.32\ \frac{m}{s}$
- $\frac{Q_D}{Q_P} = 359.9$

Figure 40: Test Hood, Cyclone Setup, and calculations for dilution ratio between isokinetic probe and fume hood

Table 10: 5x2mm, 30 SLPM

	Test 1	Test 2	Test 3	Mean	80% CI
Elapsed Time (min)	08.95	14.72	17.20	13.62	
shims (g)	100.0	82.00	83.00	88.33	
fuel (g)	479.0	470.0	477.0	475.3	
Char (g)	52.50	49.00	80.00	60.50	
PM (mgPM/kgFuel)	968.1	1263.6	1416.1	1215.9	± 284
EC (mgEC/kgFuel)	253.51	283.04	296.07	277.54	± 23.7
OC (mgOC/kgFuel)	128.48	205.85	246.39	193.57	± 65.2
EC/OC	1.97	1.37	1.20	1.52	± 0.44

Table 11: 5x2mm, 60 SLPM

	Test 1	Test 2	Test 3	Mean	80% CI
Elapsed Time (min)	12.40	12.65	12.32	12.46	
shims (g)	99.50	104.0	104.0	102.5	
fuel (g)	443.5	472.0	446.5	454.0	
Char (g)	37.00	43.50	56.50	46.67	
PM (mgPM/min)	413.2	490.7	1355.1	753.0	± 569.2
EC (mgEC/kgFuel)	39.68	53.67	88.56	60.64	± 27.4
OC (mgOC/kgFuel)	42.03	79.40	304.12	141.8	± 154.3
EC/OC	0.94	0.68	0.29	0.64	± 0.36

Table 12: 5x2mm, 90 SLPM

	Test 1	Test 2	Test 3	Mean	80% CI
Elapsed Time (min)	12.73	14.75	13.37	13.62	
shims (g)	100.0	102.0	68.00	90.00	
fuel (g)	438.0	471.5	455.0	454.8	
Char (g)	31.00	52.50	33.50	39.00	
PM (mgPM/ kgFuel)	1027.7	1853.7	1296.3	1392.6	± 458.7
EC (mgEC/kgFuel)	61.82	115.98	87.58	88.46	± 29.5
OC (mgOC/kgFuel)	97.63	469.9	303.4	290.3	± 106.5
EC/OC	0.63	0.25	0.29	0.39	± 0.17

Table 13: 5x2mm, 120 SLPM

	Test 1	Test 2	Test 3	Mean	80% CI
Elapsed Time (min)	08.95	10.90	09.98	09.94	
shims (g)	100.0	106.0	103.0	103.0	
fuel (g)	479.0	444.0	476.0	466.3	
Char (g)	52.50	32.50	16.50	33.83	
PM (mgPM/ kgFuel)	729.1	1248.0	1292.9	1089.9	± 341.1
EC (mgEC/kgFuel)	67.67	79.82	47.49	65.0	± 17.8
OC (mgOC/kgFuel)	133.36	326.75	204.28	221.5	± 106.5
EC/OC	0.51	0.24	0.23	0.33	± 0.17

Table 14: 5x3mm, 30 SLPM

	Test 1	Test 2	Test 3	Mean	80% CI
Elapsed Time (min)	16.57	16.22	16.68	16.49	
shims (g)	81.50	84.00	82.00	82.50	
fuel (g)	463.5	467.5	457.5	462.8	
Char (g)	58.00	51.50	49.50	53.00	
PM (mgPM/ kgFuel)	1016.7	1043.8	1601.9	1220.8	± 359.6
EC (mgEC/kgFuel)	165.88	299.2	360.45	275.2	± 108.3
OC (mgOC/kgFuel)	184.73	154.30	229.62	189.5	± 41.3
EC/OC	0.90	1.94	1.57	1.47	± 0.57

Table 15: 5x3mm, 60 SLPM

	Test 1	Test 2	Test 3	Test 4	Mean	80% CI
Elapsed Time (min)	16.18	17.32	13.88	16.23	15.90	
shims (g)	82.50	94.00	94.50	88.00	89.75	
fuel (g)	463.0	479.5	446.0	450.5	459.8	
Char (g)	66.50	59.50	59.50	46.50	58.00	
PM (mgPM/ kgFuel)	1548.6	1428.4	2532.7	975.0	1621.2	± 537.2
EC (mgEC/kgFuel)	314.27	303.00	259.17	255.75	283.05	± 24.50
OC (mgOC/kgFuel)	247.46	239.46	655.38	125.98	317.07	± 190.2
EC/OC	1.27	1.27	0.40	2.03	1.24	± 0.55

Table 16: 5x3mm, 90 SLPM

	Test 1	Test 2	Test 3	Mean	80% CI
Elapsed Time (min)	14.33	13.67	12.00	13.33	
shims (g)	106.0	79.50	86.00	85.33	
fuel (g)	479.5	482.0	460.0	469.5	
Char (g)	71.50	56.50	47.00	52.50	
PM (mgPM/ kgFuel)	1185.8	824.90	536.20	849.0	± 354.35
EC (mgEC/kgFuel)	247.96	183.99	118.13	183.36	± 70.70
OC (mgOC/kgFuel)	353.80	110.28	59.19	174.42	± 171.4
EC/OC	0.70	1.67	2.00	1.45	± 0.73

Table 17: 5x3mm, 120 SLPM

	Test 1	Test 2	Test 3	Mean	80% CI
Elapsed Time (min)	11.30	10.07	09.85	10.41	
shims (g)	82.00	98.00	76.00	85.33	
fuel (g)	481.0	470.0	457.5	469.5	
Char (g)	33.00	63.00	61.50	52.50	
PM (mgPM/ kgFuel)	680.1	482.4	557.4	573.3	± 73.82
EC (mgEC/kgFuel)	72.54	75.99	66.96	71.83	± 5.00
OC (mgOC/kgFuel)	52.69	52.92	110.87	72.16	± 36.5
EC/OC	1.38	1.44	0.60	1.14	± 0.51

Table 18: 16x3mm, 30 SLPM

	Test 1	Test 2	Test 3	Mean	80% CI
Elapsed Time (min)	14.42	15.13	18.23	15.93	
shims (g)	83.00	93.50	98.00	91.50	
fuel (g)	437.0	475.0	484.0	465.3	
Char (g)	64.50	67.00	55.00	62.12	
PM (mgPM/ kgFuel)	1217.4	1348.5	1107.1	1224.3	± 131.55
EC (mgEC/kgFuel)	340.34	309.14	293.68	314.39	± 25.9
OC (mgOC/kgFuel)	150.90	211.34	135.15	165.79	± 43.8
EC/OC	2.26	1.46	2.17	1.96	± 0.47

Table 19: 16x3mm, 60 SLPM

	Test 1	Test 2	Test 3	Mean	80% CI
Elapsed Time (min)	22.42	15.62	14.28	10.77	
shims (g)	83.50	90.50	103.0	92.30	
fuel (g)	463.0	448.0	477.0	462.7	
Char (g)	53.00	48.50	73.50	58.33	
PM (mgPM/ kgFuel)	2662.8	763.9	838.3	1421.7	± 1170.8
EC (mgEC/kgFuel)	458.92	198.77	275.12	310.94	± 145.6
OC (mgOC/kgFuel)	564.73	110.37	118.45	264.52	± 283.1
EC/OC	0.81	1.80	2.32	1.65	± 0.83

Table 20: 16x3mm, 90 SLPM

	Test 1	Test 2	Test 3	Mean	80% CI
Elapsed Time (min)	18.18	16.88	12.27	15.78	
shims (g)	88.00	98.00	99.00	95.00	
fuel (g)	461.0	452.0	444.5	452.5	
Char (g)	66.00	85.00	68.00	43.00	
PM(mgPM/ kgFuel)	2135.6	1934.2	934.7	1668.2	± 700.17
EC (mgEC/kgFuel)	440.70	420.13	282.32	381.05	± 93.8
OC (mgOC/kgFuel)	412.80	516.14	77.13	335.36	± 249.9
EC/OC	1.07	0.81	3.66	1.85	± 1.71

Table 21: 16x3mm, 120 SLPM

	Test 1	Test 2	Test 3	Mean	80% CI
Elapsed Time (min)	15.92	12.75	14.23	14.30	
shims (g)	97.00	94.00	103.0	98.00	
fuel (g)	484.0	452.5	464.0	466.8	
Char (g)	58.50	65.00	53.50	59.00	
PM (mgPM/ kgFuel)	1051.7	850.9	673.5	858.7	± 205.96
EC (mgEC/kgFuel)	197.52	195.44	169.56	187.5	± 17.0
OC (mgOC/kgFuel)	205.12	138.75	86.35	143.4	± 64.8
EC/OC	0.96	1.41	1.96	1.45	± 0.55

Table 22: EGR EC/OC Results

	Test 1	Test 2	Test 3	Mean	80% CI
Elapsed Time (min)	16.03	15.27	15.55	15.62	
shims (g)	105.5	106.0	100.0	103.8	
fuel (g)	451.0	482.5	461.0	464.8	
Char (g)	53.50	73.50	53.50	60.12	
PM(mgPM/ kgFuel)	1762.2	844.97	957.59	1188.2	± 544.57
EC (mgEC/kgFuel)	387.11	206.35	258.78	284.1	± 101.24
OC (mgOC/kgFuel)	293.61	121.94	112.99	176.18	± 110.82
EC/OC	1.32	1.69	2.29	1.77	± 0.53

Table 23: Baseline EC/OC Results

	Test 1	Test 2	Test 3	Mean	80% CI
Elapsed Time (min)	15.08	15.63	12.27	14.33	
shims (g)	89.5	90	89	89.5	
fuel (g)	459	462.5	444	455.2	
Char (g)	60	41	61.5	54.2	
PM(mgPM/ kgFuel)	4187.4	4821.4	6152.5	5053.8	± 1091.9
EC (mgEC/kgFuel)	747.97	1143.3	2012.3	1301.2	± 704.13
OC (mgOC/kgFuel)	1021.8	947.95	415.66	795.14	± 360.02
EC/OC	0.73	1.21	4.84	2.26	± 2.45

Table 24: Approximate nozzle velocities for each operating condition tested, assuming T = 600°C upon exiting the nozzle

Velocities (m/s)			
Flow (SLPM)	5x2mm	5x3mm	16x3mm
30	76	34	11
60	144	68	21
90	198	100	32
120	236	130	43

Table 25: Throat Re Numbers for each operating condition tested using velocities found in Table 24

Throat Re Numbers			
Flow (SLPM)	5x2mm	5x3mm	16x3mm
30	47,291	21,019	6,569
60	94,593	42,039	13,139
90	141,890	63,068	19,707
120	189,188	84,090	26,275

Table 26: Two-Factor With Replication ANOVA Table for Total EC

SUMMARY	5x2mm	5x3mm	16x3mm	Total		
30						
Count	3	3	3	9		
Sum	832.6101005	825.533634	943.1611745	2601.304909		
Average	277.5367002	275.177878	314.3870582	289.0338788		
Variance	475.5645227	9897.118076	564.9348639	3097.013458		
60						
Count	3	3	3	9		
Sum	181.9127845	817.9183995	932.8119486	1932.643133		
Average	60.63759482	272.6394665	310.9373162	214.7381258		
Variance	633.8433855	694.3122167	17880.54692	18434.85931		
90						
Count	3	3	3	9		
Sum	265.376613	550.0724658	1143.155262	1958.604341		
Average	88.458871	183.3574886	381.051754	217.6227045		
Variance	733.7964089	4214.438653	7416.824163	19803.68547		
120						
Count	3	3	3	9		
Sum	194.9779108	215.4950512	562.5203011	972.9932632		
Average	64.99263695	71.83168375	187.506767	108.1103626		
Variance	266.581623	20.78894264	242.6287064	3687.151009		
Total						
Count	12	12	12			
Sum	1474.877409	2409.01955	3581.648686			
Average	122.9064507	200.7516292	298.4707238			
Variance	9200.480181	10231.22038	10075.81681			
ANOVA	alpha = 0.20	TOTAL EC				
Source of Variation	*SS*	*df*	*MS*	*F*	*P-value*	*F crit*
flow rate	150127.8461	3	50042.61537	13.9519552	1.80105E-05	1.669944344
nozzle	185726.829	2	92863.41451	25.89045735	1.01816E-06	1.722358033
Interaction	88372.08798	6	14728.68133	4.106378145	0.005645064	1.566699807
Within	86082.75697	24	3586.78154			
Total	510309.5201	35				

Table 27: Two-Factor With Replication ANOVA Table for Total OC

SUMMARY	5x2mm	5x3mm	16x3mm	Total		
30						
Count	3	3	3	9		
Sum	580.7146793	568.6411708	497.3791234	1646.734974		
Average	193.5715598	189.5470569	165.7930411	182.9705526		
Variance	3588.896728	1435.89258	1617.67367	1829.627743		
60						
Count	3	3	3	9		
Sum	425.5490041	1020.818114	793.5489325	2239.916051		
Average	141.849668	340.2727046	264.5163108	248.8795612		
Variance	20098.39838	77687.89471	67612.64806	48869.46502		
90						
Count	3	3	3	9		
Sum	870.9277441	523.2691032	1006.073334	2400.270182		
Average	290.309248	174.4230344	335.3577781	266.6966868		
Variance	34774.5807	24784.30603	52681.26962	33229.91113		
120						
Count	3	3	3	9		
Sum	664.3906744	216.4728346	430.2142498	1311.077759		
Average	221.4635581	72.15761153	143.4047499	145.6753065		
Variance	9571.160295	1123.724991	3542.964983	7742.162313		
Total						
Count	12	12	12			
Sum	2541.582102	2329.201222	2727.21564			
Average	211.7985085	194.1001019	227.26797			
Variance	15501.20966	29090.59913	29323.47899			
ANOVA	alpha = 0.20	TOTAL OC				
Source of Variation	*SS*	*df*	*MS*	*F*	*P-value*	*F crit*
flow rate	86309.41719	3	28769.80573	1.1564999	0.346788496	1.669944344
nozzle	6610.58125	2	3305.290625	0.132867365	0.876220789	1.722358033
Interaction	129719.9269	6	21619.98782	0.869088724	0.531638869	1.566699807
Within	597038.8215	24	24876.61756			
Total	819678.7468	35				

Table 28: Two-Factor With Replication ANOVA Table for Total EC/OC

SUMMARY	5x2mm	5x3mm	16x3mm	Total		
30						
Count	3	3	3	9		
Sum	4.549769517	4.406896175	5.891313313	14.84797901		
Average	1.516589839	1.468965392	1.963771104	1.649775445		
Variance	0.163865276	0.278603092	0.18995394	0.21398956		
60						
Count	3	3	3	9		
Sum	1.911278546	3.690860086	4.936325638	10.53846427		
Average	0.637092849	1.230286695	1.645441879	1.170940474		
Variance	0.107701288	0.668901101	0.588256715	0.533839843		
90						
Count	3	3	3	9		
Sum	1.168690191	4.364965689	5.541884583	11.07554046		
Average	0.389563397	1.454988563	1.847294861	1.230615607		
Variance	0.044963109	0.453359766	2.481332311	1.171665801		
120						
Count	3	3	3	9		
Sum	0.98416451	3.416823244	4.335245887	8.736233641		
Average	0.328054837	1.138941081	1.445081962	0.970692627		
Variance	0.024156253	0.215525386	0.251365292	0.372637775		
Total						
Count	12	12	12			
Sum	8.613902765	15.87954519	20.70476942			
Average	0.71782523	1.323295433	1.725397452			
Variance	0.308548189	0.316034418	0.681069859			
ANOVA	alpha = 0.20	EC/OC				
Source of Variation	*SS*	*df*	*MS*	*F*	*P-value*	*F crit*
flow rate	2.199041215	3	0.733013738	1.608667036	0.213539533	1.669944344
nozzle	6.173927925	2	3.086963962	6.77463042	0.004648557	1.722358033
Interaction	1.227168852	6	0.204528142	0.44885609	0.838571132	1.566699807
Within	10.93596706	24	0.455665294			
Total	20.53610505	35				

Table 29: Two-Factor With Replication ANOVA Table for Percent EC

SUMMARY	5x2mm	5x3mm	16x3mm	Total		
30						
Count	3	3	3	9		
Sum	1.788391252	1.743752809	1.971625538	5.503769599		
Average	0.596130417	0.581250936	0.657208513	0.611529955		
Variance	0.003694839	0.009365524	0.003016932	0.005234509		
60						
Count	3	3	3	9		
Sum	1.114485413	1.511925633	1.790337041	4.416748086		
Average	0.371495138	0.503975211	0.596779014	0.490749787		
Variance	0.017671956	0.039598394	0.017317113	0.028261408		
90						
Count	3	3	3	9		
Sum	0.809666813	1.703489234	1.750495622	4.263651669		
Average	0.269888938	0.567829745	0.583498541	0.473739074		
Variance	0.010581218	0.018618198	0.0317228	0.038651206		
120						
Count	3	3	3	9		
Sum	0.721560839	1.545311978	1.737968156	4.004840972		
Average	0.24052028	0.515103993	0.579322719	0.44498233		
Variance	0.006938666	0.014425263	0.007420232	0.03148446		
Total						
Count	12	12	12			
Sum	4.434104317	6.504479652	7.250426357			
Average	0.369508693	0.542039971	0.604202196			
Variance	0.028322158	0.016104183	0.011881033			
ANOVA	alpha = 0.20	PERCENT EC OF TOTAL C				
Source of Variation	*SS*	*df*	*MS*	*F*	*P-value*	*F crit*
flow rate	0.14517734	3	0.048392447	3.219524876	0.040591223	1.669944344
nozzle	0.354848899	2	0.177424449	11.80395842	0.000269392	1.722358033
Interaction	0.113461499	6	0.01891025	1.258089313	0.313165914	1.566699807
Within	0.360742272	24	0.015030928			
Total	0.97423001	35				

Table 30: Raw test results for Total EC

Total EC (mg/kgFuel)			
Flow (SLPM)	5x2mm	5x3mm	16x3mm
30	253.51	165.88	340.34
	283.04	299.20	309.14
	296.07	360.45	293.68
60	39.68	255.75	458.92
	53.67	303.00	198.77
	88.56	259.17	275.12
90	61.82	247.96	440.70
	115.98	183.99	420.13
	87.58	118.13	282.32
120	67.67	72.54	197.52
	79.82	75.99	195.44
	47.49	66.96	169.56

Table 31: Raw test results for Total OC

Total OC (mg/kgFuel)			
Flow (SLPM)	5x2mm	5x3mm	16x3mm
30	128.48	184.73	150.90
	205.85	154.30	211.34
	246.39	229.62	135.15
60	42.03	125.98	564.73
	79.40	239.46	110.37
	304.12	655.38	118.45
90	97.63	353.80	412.80
	469.90	110.28	516.14
	303.40	59.19	77.13
120	133.36	52.69	205.12
	326.75	52.92	138.75
	204.28	110.87	86.35

Table 32: Raw test results for EC/OC

EC/OC			
Flow (SLPM)	5x2mm	5x3mm	16x3mm
30	1.97	0.90	2.26
	1.37	1.94	1.46
	1.20	1.57	2.17
60	0.94	2.03	0.81
	0.68	1.27	1.80
	0.29	0.40	2.32
90	0.63	0.70	1.07
	0.25	1.67	0.81
	0.29	2.00	3.66
120	0.51	1.38	0.96
	0.24	1.44	1.41
	0.23	0.60	1.96

Table 33: Raw test results for percent EC of total C

Percent EC (mgEC/kgFuel)			
Flow (SLPM)	5x2mm	5x3mm	16x3mm
30	66.4%	47.3%	69.3%
	57.9%	66.0%	59.4%
	54.6%	61.1%	68.5%
60	48.6%	67.0%	44.8%
	40.3%	55.9%	64.3%
	22.6%	28.3%	69.9%
90	38.8%	41.2%	51.6%
	19.8%	62.5%	44.9%
	22.4%	66.6%	78.5%
120	33.7%	57.9%	49.1%
	19.6%	58.9%	58.5%
	18.9%	37.7%	66.3%

$$\Delta p = \frac{\rho}{2}\left(\frac{Q}{C_d A_{orifice}}\right)^2 (1-\beta^4)$$

$$C_d = f(\beta) + 91.71\beta^{2.5}Re^{-0.75} + \frac{0.09\beta^4}{1-\beta^4}F_1 - 0.0337\beta^3 F_2$$

$$F_1 = 0.4333$$

$$F_2 = 0.47$$

$$f(\beta) = 0.5959 + 0.0312\beta^{2.1} - 0.184\beta^8$$

$$\beta = \frac{D_{orifice}}{D_{tube}}$$

$$Re = \frac{V_{tube} D_{tube}}{\nu}$$

Assumptions:

D_{tube} = 0.0381m

T_{air} = 300 K

Thermophysical Properties:

$$\rho_{air} = 1.1614\ \frac{kg}{m^3}$$

$$\nu = 15.89 * 10^{-6}\frac{m^2}{s}$$

Figure 41: Equations used for calculating the pressure drop across the nozzle/orifices (White, 1999)

Table 34: Calculated values used for prototype system curve

LPM	Q [m^3/s]	$V_{orifice}$ [m/s]	Re	Cd	Orifice dP [Pa]
20	0.0003	2.9	701	0.597	14.20
40	0.0007	5.9	1402	0.597	56.70
60	0.0010	8.8	2103	0.597	127.7
80	0.0013	11.8	2804	0.596	227.1
100	0.0017	14.7	3505	0.596	355.0
120	0.0020	17.7	4206	0.596	511.2
140	0.0023	20.6	4907	0.596	695.8
160	0.0027	23.6	5608	0.596	908.9

$$\tau = \frac{\rho_p d_p^2 C_c}{18\eta}$$

Where:

$\rho_p \equiv particle\ density = 1900\ \left[\frac{kg}{m^3}\right]$ (Schnieder, et al., 2006)

$d_p \equiv particle\ diameter = 0.2\ [\mu m]$ (L'Orange, Volckens, & DeFoort, Influence of stove type and cooking pot temperature on particulate matter emissions from biomass cook stoves, 2012)

$$C_c \equiv Cunningham\ Correction\ factor = 1 + \frac{2.52\lambda}{d_p}$$

$$\lambda \equiv mean\ free\ path\ of\ air\ molecule = 66\ [nm]$$

$$\eta \equiv dynamic\ viscosity = 1.8134 \times 10^{-5}[Pa \cdot s]$$

Equation 9: Relaxation time for Stokes number, 3.6.2 (Hinds, 1999)

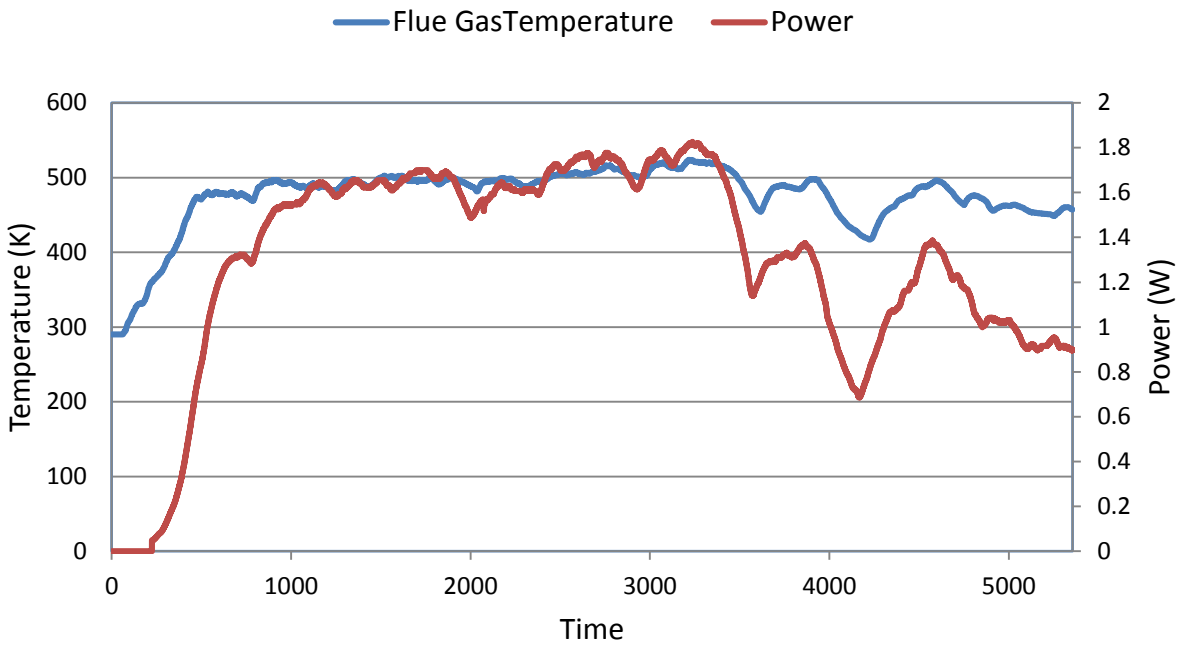

Figure 42: 3-Fin Heat Sink with CPU Cooler: Constant Resistance at 2.9 Ω

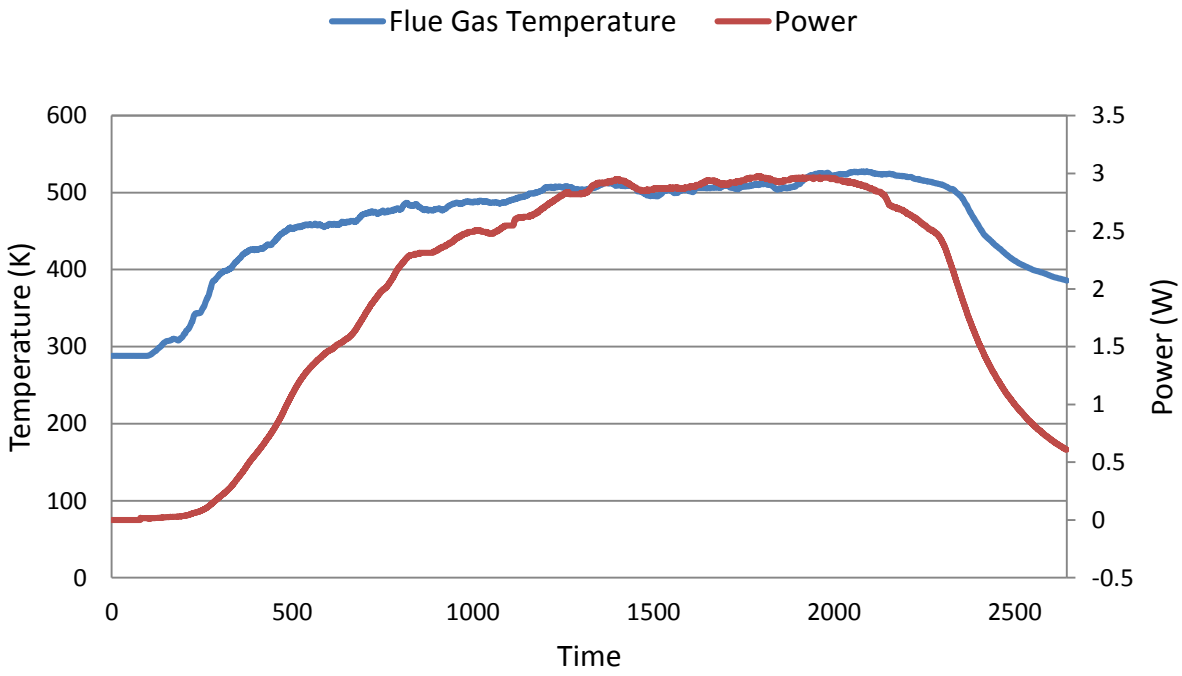

Figure 43: 3-Fin Heat Sink with H_2O Block: Constant Resistance at 2.9 Ω

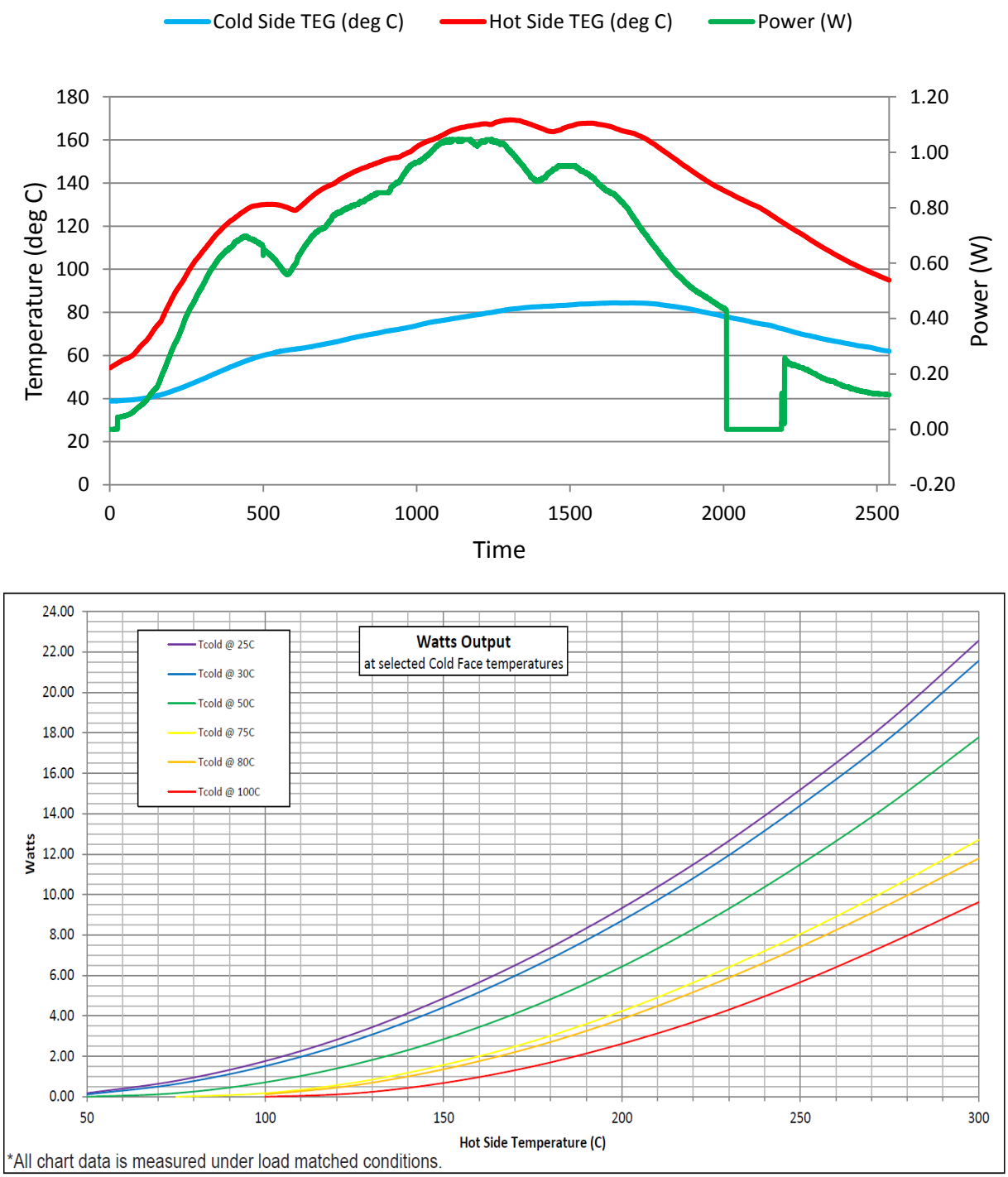

Figure 44: Top - Field prototype power output and dT, Bottom - Custom Thermoelectric power output specifications for the 2411G-7L31-15CX1 module (Custom Thermoelectric, 2014)

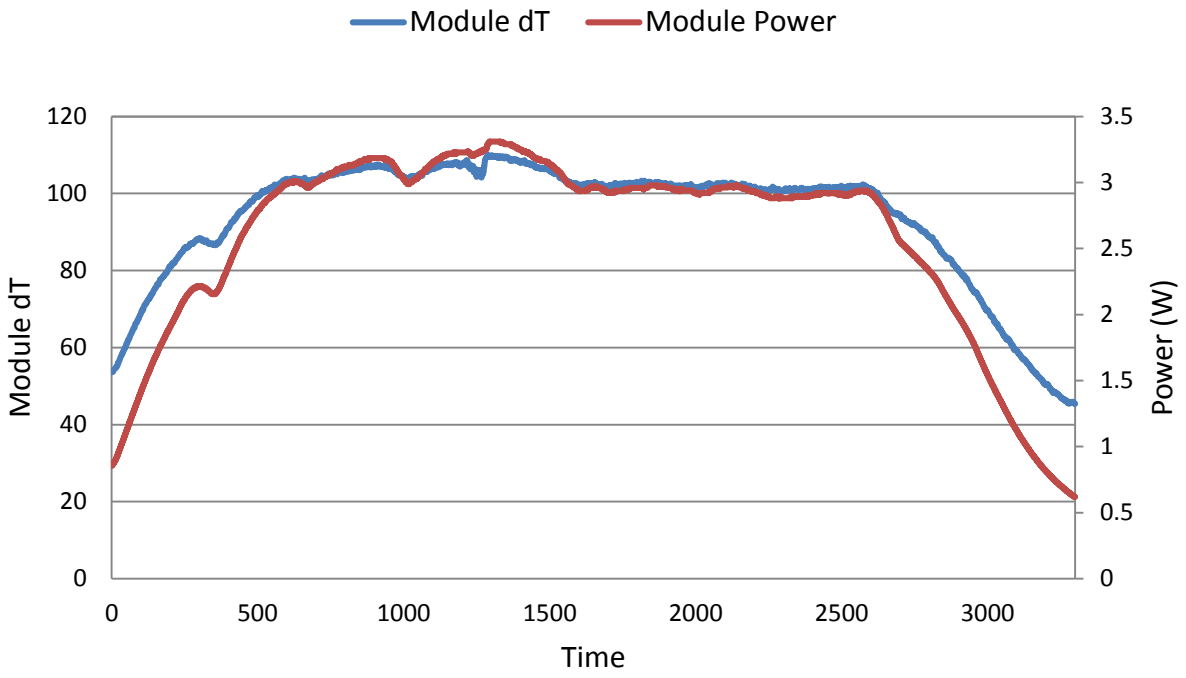

Figure 45: Laboratory prototype TEG power module test results; single elliptical fin used for heat capture and water block used for heat rejection

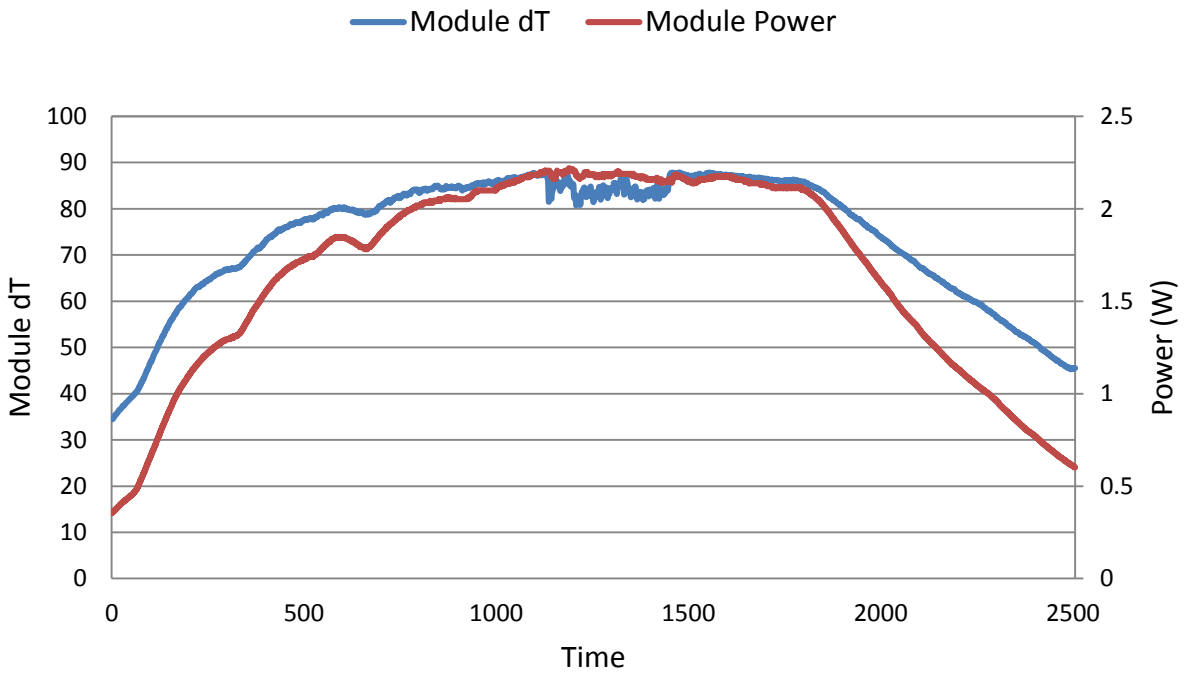

Figure 46: Laboratory prototype TEG power module with 60 SLPM forced air injection test results; single elliptical fin used for heat capture and water block used for heat rejection

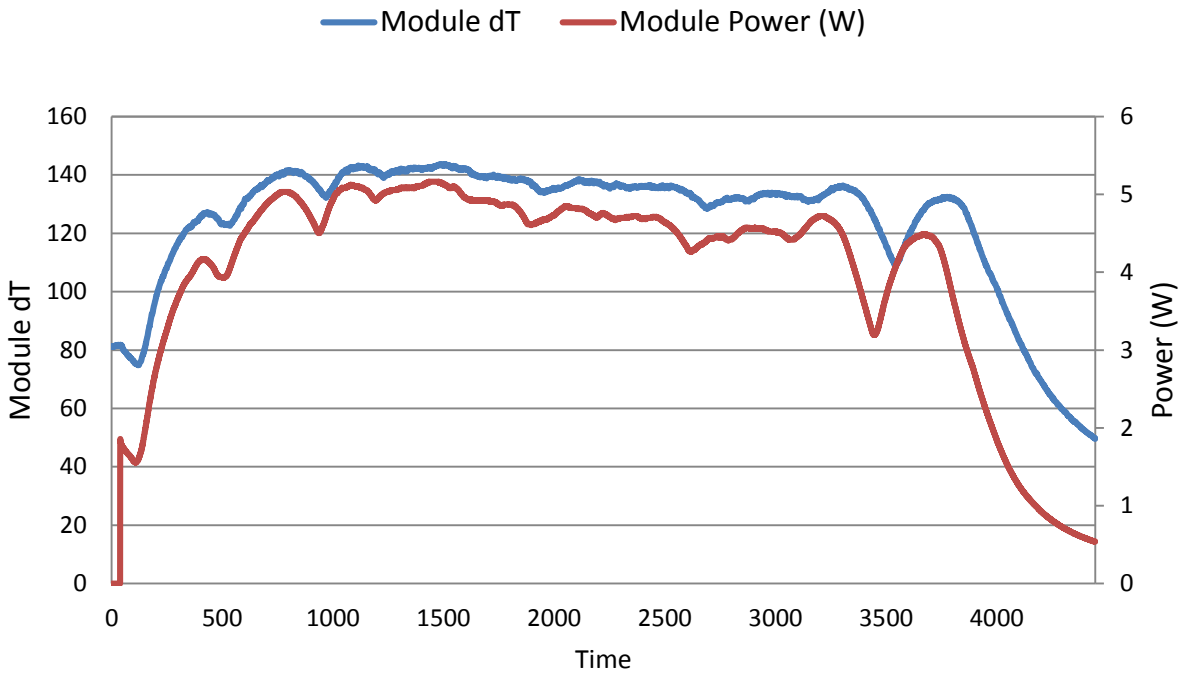

Figure 47: Laboratory prototype TEG power module test results; 3-fin heat sink used for heat capture and water block used for heat rejection

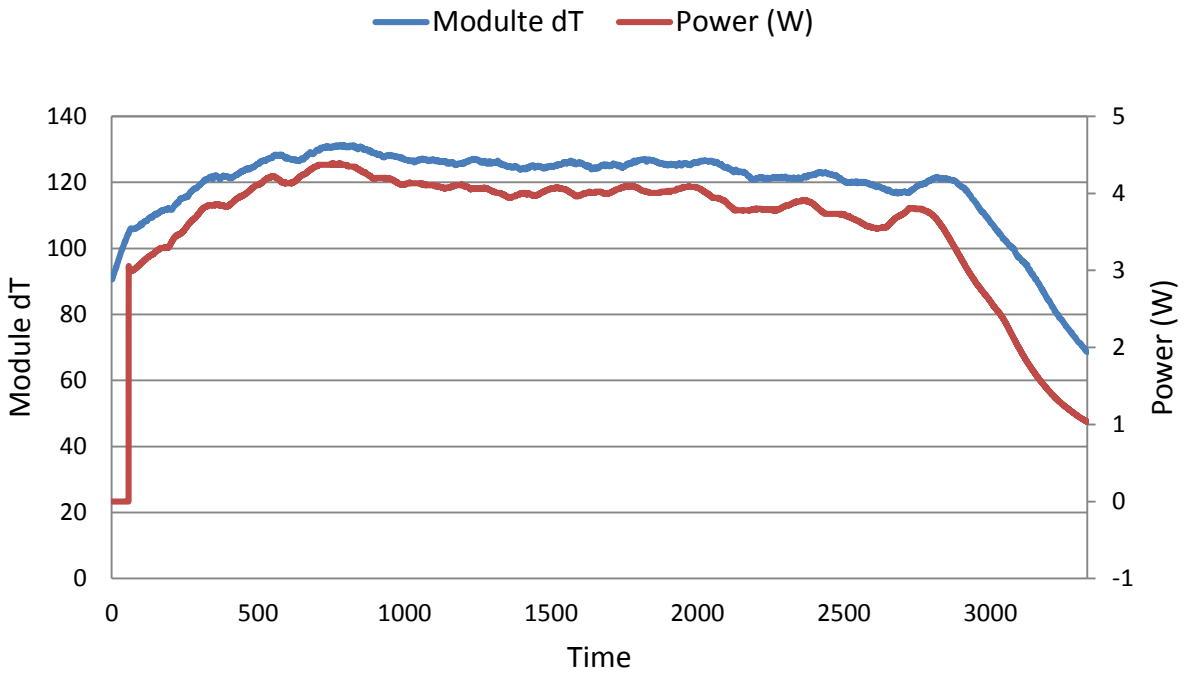

Figure 48: Laboratory prototype TEG power module with 60 SLPM forced air injection test results; 3-fin heat sink used for heat capture and water block used for heat rejection

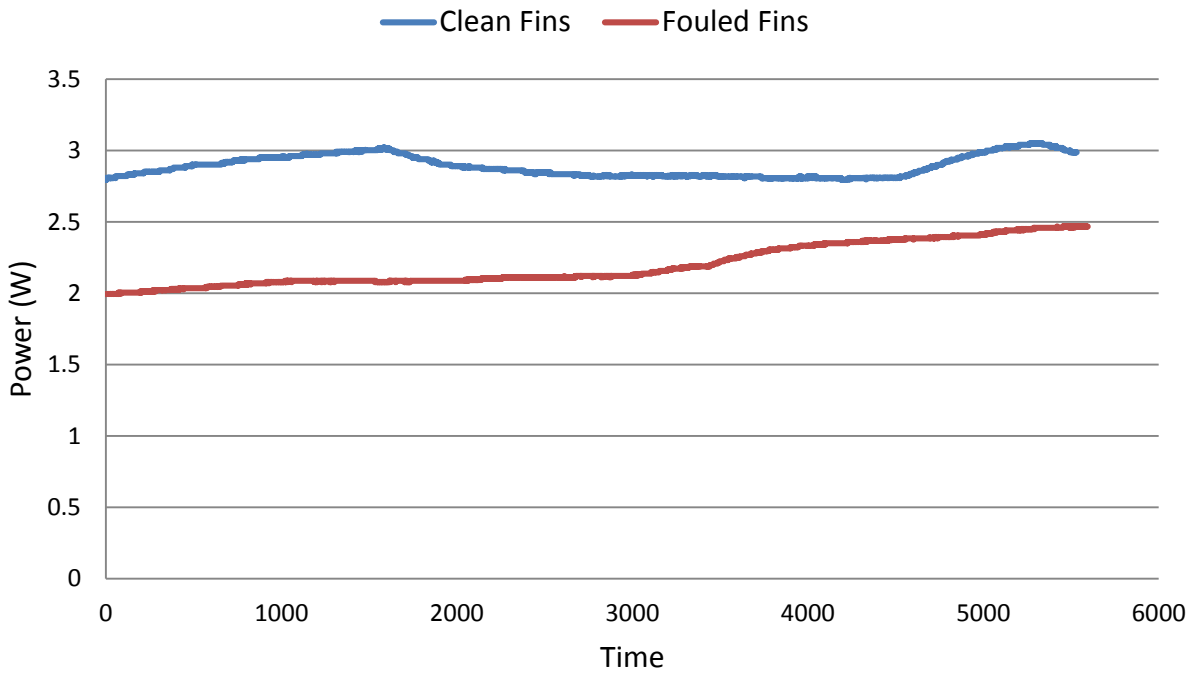

Figure 49: TEG power module test results with fouling from 7 hours of high firepower exposure compared to clean fins. Both tests were completed with a propane torch so that additional fouling did not occur.

Figure 50: A propane torch was used for testing the effects of fouling on the heat capture heat sink in the TEG power module. Using a propane torch prevented the accumulation of additional soot during the test.